

THE DISRUPTION OF GIANT MOLECULAR CLOUDS BY RADIATION PRESSURE
& THE EFFICIENCY OF STAR FORMATION IN GALAXIES

NORMAN MURRAY^{1,2}, ELIOT QUATAERT³, & TODD A. THOMPSON^{4,5,6}

Draft version June 29, 2009

ABSTRACT

Star formation is slow, in the sense that the gas consumption time is much longer than the dynamical time. It is also inefficient; essentially all star formation in local galaxies takes place in giant molecular clouds (GMCs), but the fraction of a GMC converted to stars is very small, $\sim 5\%$. While there is some disagreement over the lifespan of GMCs, there is a consensus that it is no more than a few cloud dynamical times. In the most luminous starbursts, the GMC lifetime is shorter than the main sequence lifetime of even the most massive stars, so that supernovae can play no role in GMC disruption; another feedback mechanism must dominate. We investigate the disruption of GMCs across a wide range of galaxies, from normal spirals to the densest starbursts; we take into account the effects of HII gas pressure, shocked stellar winds, protostellar jets, and radiation pressure produced by the absorption and scattering of starlight on dust grains. In the Milky Way, we find that a combination of three mechanisms — jets, HII gas pressure, and radiation pressure — disrupts the clouds. In more rapidly star forming galaxies such as “clump” galaxies at high-redshift, ultra-luminous infrared galaxies (ULIRGs) and submillimeter galaxies, radiation pressure dominates natal cloud distribution. We predict the presence of ~ 10 – 20 clusters with masses $\sim 10^7 M_\odot$ in local ULIRGs such as Arp 220 and a similar number of clusters with $M_* \sim 10^8 M_\odot$ in high redshift clump galaxies; submillimeter galaxies will have even more massive clusters. We find that the mass fraction of a GMC that ends up in stars is an increasing function of the gas surface density of a galaxy, reaching $\sim 35\%$ in the most luminous starbursts. Furthermore, the disruption of bubbles by radiation pressure stirs the interstellar medium to velocities of $\sim 10 \text{ km s}^{-1}$ in normal galaxies and to $\sim 100 \text{ km s}^{-1}$ in ULIRGs like Arp 220, consistent with observations. Thus, radiation pressure may play a dominant role in the ISM of star-forming galaxies.

Subject headings: Galaxies: star clusters, formation, general, starburst — HII regions — ISM: clouds, bubbles — stars: formation

1. INTRODUCTION

The Kennicutt law (Kennicutt 1998)

$$\dot{\Sigma}_* = \eta \Sigma_g \Omega \quad (1)$$

relates the star formation surface density $\dot{\Sigma}_*$ to the gas surface density Σ_g and the local dynamical time $\Omega \approx v_c/R$ in disk galaxies, where v_c is the circular velocity of the galaxy and R is the distance from the galactic center. The dimensionless constant $\eta \approx 0.017$ is surprisingly small, a finding that is interpreted as showing that star formation is a slow process. Star formation is similarly slow on smaller scales within galaxies (Kennicutt et al. 2007; Bigiel et al. 2008; Leroy et al. 2008; Krumholz & Tan 2007).

Remarkably, equation (1) holds for galaxies like the Milky Way, with rather modest star formation rates of order a solar mass per year, for starburst galaxies with star formation

rates of order tens of solar masses per year, for ultraluminous infrared galaxies (ULIRGs) with star formation rates around one hundred solar masses per year, and for sub-millimeter galaxies with star formation rates in excess of one thousand solar masses per year. There are indications, however, that the star formation efficiency η may be larger in ULIRGs and sub-mm galaxies, with $\eta \sim 0.1$ (Bouché et al. 2007).

The large range of galaxies that obey equation (1) suggests that whatever process sets the efficiency of star formation operates in galaxies with very different conditions in their interstellar media. For example, the gas surface density in the Milky Way at 8 kpc is $\Sigma_g \approx 2 \times 10^{-3} \text{ g cm}^{-2}$ (Boulares & Cox 1990), while that in the two 100 pc star forming disks of the ultra-luminous infrared galaxy (ULIRG) Arp 220 is $\Sigma_g \approx 7 \text{ g cm}^{-2}$; the mean gas densities of the two galaxy’s star forming disks also differ by a factor of $\gtrsim 10^4$. Although the range in turbulent velocities in the ISM is not so dramatic, from $\sim 6 \text{ km s}^{-1}$ in the Milky Way to ~ 60 – 80 km s^{-1} in Arp 220 (Downes & Solomon 1998), the turbulent pressure in Arp 220 exceeds that in the Galaxy by a factor of $\sim 10^6$.

Another signature of inefficient star formation relates to individual giant molecular clouds (GMCs). In the Milky Way, all stars are believed to form in such clouds. However, the fraction ϵ_{GMC} of a GMC that is turned into stars is quite low, around 5% in the Milky Way (Williams & McKee 1997; Evans et al. 2008), with a similar value inferred from the global star formation efficiencies in other galaxies (see,

¹ Canada Research Chair in Astrophysics

² Canadian Institute for Theoretical Astrophysics, 60 St. George Street, University of Toronto, Toronto, ON M5S 3H8, Canada; murray@cita.utoronto.ca

³ Astronomy Department & Theoretical Astrophysics Center, 601 Campbell Hall, The University of California, Berkeley, CA 94720; eliot@astro.berkeley.edu

⁴ Department of Astronomy, The Ohio State University, 140 W 18th Ave., Columbus, OH 43210; thompson@astronomy.ohio-state.edu.

⁵ Center for Cosmology & Astro-Particle Physics, The Ohio State University, 191 W. Woodruff Ave., Columbus, OH 43210

⁶ Alfred P. Sloan Fellow

e.g., McKee & Ostriker 2007).

One class of explanation for this low star formation efficiency is that gas in the ISM is prevented from collapsing by, for example, magnetic fields, cosmic rays, or by externally-driven turbulence (Parker 1969; Sellwood & Balbus 1999; Ostriker, Stone, & Gammie 2001). A second class of explanation is known by the name of “feedback:” the injection of energy and momentum into the ISM by stellar processes so that star formation alters the ISM conditions and limits the rate at which gas turns into stars. The form the feedback takes is not currently agreed upon. Suggested mechanisms include supernova heating, deposition of momentum by supernovae, heating by photoionizing radiation from massive stars, deposition of momentum by expanding bubbles of photoionized HII region gas, deposition of momentum by the shocked winds from massive stars, and jets from protostars (e.g., McKee & Ostriker 1977; Silk 1997; Wada & Norman 2001; Matzner 2002; Li & Nakamura 2006; Cunningham et al. 2008).

In this paper, we study these feedback processes and assess the role that they play in disrupting GMCs across a wide range of star-forming galaxies. In addition, we focus on a somewhat less well studied form of feedback: deposition of momentum by the absorption and scattering of starlight by dust grains (O’Dell et al. 1967; Chiao & Wickramasinghe 1972; Elmegreen 1983; Ferrara 1993; Scoville et al. 2001; Scoville 2003; Thompson et al. 2005). Although the magnetic fields in starburst galaxies can be large (\sim few mG for Arp 220; Thompson et al. 2006, Robishaw et al. 2008), we neglect them throughout this paper in order to focus on the competition between various processes that contribute to disrupting GMCs.

It is important to distinguish between two arenas in which galactic feedback likely operates: galactic disks in the large, and in the main units of star formation, GMCs. While there is rather sharp debate in the literature, we will assume that GMCs are at least marginally gravitationally bound objects, and hence that they are unlikely to be supported by feedback acting on the scale of galactic disks as a whole. As noted above, observations in our own and nearby galaxies establish that only $\sim 5\%$ of the gas in a GMC ends up in stars; the rest of the gas is dispersed back into the ISM. The universality of the Kennicutt law suggests that a similarly small fraction of the GMCs in other, more distant classes of galaxies, is turned into stars. Something is disrupting GMCs, but it is unlikely to be large scale turbulence in the galaxy as a whole. Instead, GMCs must be disrupted by the stars that form in them. A number of authors have argued that galactic GMCs are disrupted by expanding HII regions (e.g., Matzner 2002; Krumholz et al. 2006); this mechanism cannot, however, work in luminous starbursts (Matzner 2002). The fact that these galaxies nonetheless have roughly similar star formation efficiencies suggests that another disruption mechanism must be competitive with expanding HII regions.

In this paper, we argue that the radiation pressure produced by the largest few star clusters in a GMC, acting on dust grains in the gas, is the primary mechanism by which GMCs are disrupted in more luminous starbursts and massive GMCs (see also Scoville et al. 2001, Harper-Clark & Murray 2009, and Pellegrini et al. 2007, 2009). Protostellar jets also provide an important contribution, particularly in the early stages of the evolution. In spirals like the Milky Way, both expanding HII regions and radiation pressure are comparably important, depending on the size and mass of the cluster, and supernovae

also play an important role in the latest stages of disruption.

1.1. *Is Feedback Really Necessary?*

A key thesis of this work is that stellar feedback is crucial for understanding the low observed values of the star formation efficiency in galaxies. In contrast, Krumholz & McKee (2005) present an explanation of the Kennicutt-Schmidt law (eq. 1) that does not invoke an explicit form of feedback. Their argument is that turbulent motions prevent the collapse of the bulk of the gas in a GMC (or in other bound objects); only if the density is above a critical density, which depends on the Mach number of the flow, do stars actually form. The fraction of gas in a turbulent flow that lies above this critical density is small, leading to the low observed star formation efficiency per dynamical time.

We find this argument to be compelling, as far as it goes. As long as turbulence is maintained, only a small fraction of gas will collapse into stars per dynamical time. However, the assumption of a constant level of turbulence is essential to the Krumholz & McKee (2005) argument. A key, and yet unanswered, question is thus *what maintains the turbulence?* If the turbulence in a GMC is not maintained, then the GMC will contract, leading to an increase in the mean density and a decrease in the dynamical time. Indeed, simulations find that turbulence decays on ~ 1 crossing time (Mac Low 1999; Ostriker et al. 2001), so that a continued source of energy is needed to maintain the turbulent support of the cloud. It is possible, in principle, that gravitational contraction of a GMC can sustain the turbulence, maintaining approximate virial equilibrium and a slow contraction of the cloud (Krumholz et al. 2006). We argue, however, that an independent internal source of turbulence, provided by stars, is crucial to maintaining the slow rate of star formation.

As an example, we apply this argument to Arp 220. The interstellar medium of Arp 220 has a turbulent Mach number $\mathcal{M} \approx 100$. The fraction of a GMC (or any bit of molecular gas) that is sufficiently dense to be converted into stars in a free fall time is then $\simeq 0.013 - 0.05$ for GMC’s with a virial parameter $\alpha_{\text{vir}} = 0.1 - 1$ (see Figure 3 of Krumholz & McKee 2005).⁷ According to this argument, a GMC will convert half its gas into stars in ten to forty free fall times, reasonably consistent with equation (1) for any α_{vir} . However, this assumes that the cloud does not collapse and reduce its free fall time. In reality, if turbulence can only maintain $\alpha_{\text{vir}} \sim 0.1$, a cloud is likely to collapse, leading to a rapid increase in density and a decrease in the free-fall time. If the star formation rate per free-fall time remains roughly constant, then the actual star formation rate will increase rapidly with time, and most of the gas in the cloud will be turned into stars in roughly one initial (large-scale) free-fall time. Thus the model of Krumholz & McKee (2005) for the low star formation efficiency in galaxies relies critically on maintaining sufficient levels of turbulence so that $\alpha_{\text{vir}} \sim 1$. On larger scales — above the characteristic GMC size — the equivalent argument is that the galactic disk must have Toomre $Q \sim 1$, as we discuss below.

1.2. *This Paper*

⁷ A virial parameter $\alpha_{\text{vir}} = 1$ corresponds to a cloud that is just gravitationally bound, while the smaller value of $\alpha_{\text{vir}} = 0.1$ corresponds to a cloud that is approaching free fall conditions.

The remainder of this paper is organized as follows. In §2, we collect a number of relevant astrophysical results used in our modeling. In §3, we describe a simple one-dimensional model for the disruption of GMCs which includes the effects of HII gas pressure, proto-stellar jets, radiation pressure, gas pressure associated with shocked stellar winds, and wind shock generated cosmic rays (many of the details of how we model these forces are given in Appendix A). In section §4 we present the results of our numerical modeling of GMC disruption in star forming galaxies. To explore the wide range of conditions seen in galaxies across the Kennicutt-Schmidt law, we consider models for GMCs in the Milky Way, M82, Arp 220, and the $z \sim 2$ galaxy Q2346-BX 482. In §5, we discuss the implications of our results, the origin of turbulence in galaxies, and explain physically why radiation pressure is the only source of stellar feedback in principle capable of disrupting GMCs across the huge dynamic range in ISM conditions from normal galaxies to the densest starbursts.

2. ASTROPHYSICAL ELEMENTS

In this section we collect several pieces of observations and physics that we believe are relevant to star formation in galactic disks and GMCs. We order these items according to the amount of support they enjoy, from substantial to slim. The key conclusion below is that a significant fraction of all stars are formed in compact (\sim few pc radius) massive star clusters, that in turn reside in GMCs. Given the importance of a few star clusters that are small compared to the GMC as a whole, a one dimensional model for GMC disruption is a reasonable first approximation; this is presented in §3.

2.1. Marginally Stable Disks ($Q \approx 1$)

Quirk (1972) showed that normal galaxies have gas disks with $Q \approx 1$. Kennicutt (1989) refined this to the statement that *within the star forming part of normal galactic disks*, $1/4 \lesssim Q \lesssim 0.6$. At large radii he found $Q > 1$ and a lack of star formation. More recently, Leroy et al. (2008) studied star formation in detail in 23 nearby galaxies. They found that if they accounted for only the gas surface density, as done above, their disks were stable, with $Q \approx 3-4$; using the total (gas plus stars) surface density resulted in $Q \approx 2$ with a slight variation in radius. Unlike Kennicutt (1989), they find that star formation occurs at large radii, beyond Kennicutt's $Q > 1$ radius, albeit at reduced rates.

These studies were restricted to normal galaxies, and employed a fixed sound speed as the estimate for the random velocity. However, there is evidence that disks with turbulent velocity $v_T \gg c_s$ also satisfy $Q \sim 1$ when v_T is used in evaluating Q (e.g., Thompson et al. 2005 and our discussion of the starbursts M82, Arp 220, and Q2346-BX 482 in §4). Motivated by these observations and by theoretical considerations, we will assume that all star forming galaxies have $Q \approx 1$.

2.2. The Toomre Mass and Giant Molecular Clouds

We assume that galactic disks initially fragment on the disk scale height $H \approx (v_T/v_c)r$. The fragments will form gravitationally bound structures with a mass given by the Toomre mass, $M_T \approx \pi H^2 \Sigma_g$. Near the location of the sun, the gas surface density $\Sigma_g \approx 2 \times 10^{-3} \text{ g cm}^{-2}$ and $H \sim 300 \text{ pc}$, giving $M_T \approx 2 \times 10^6 M_\odot$.

This scenario is consistent with observations of GMCs in our galaxy; in the Milky Way half the gas is in molecular form in giant molecular clouds with a characteristic mass of order $5 \times 10^5 M_\odot$ (Solomon et al. 1987), but with a rather wide range of masses. The number of clouds $N(m)$ of mass m is given by

$$\frac{dN}{dm} = N_0 \left(\frac{m}{m_0} \right)^{-\alpha_G}, \quad (2)$$

with an exponent $\alpha_G \sim 1.8$ (Solomon et al. 1987) or 1.6 (Williams & McKee 1997), so that most of the mass is in the largest clouds. As a cautionary note, we note that Engargiola et al. (2003) find $\alpha_G = 2.6 \pm 0.3$ in M33, which suggests that lower mass clouds contribute a significant fraction of the total mass. In the Milky Way the largest GMCs have masses of order $\sim 3 \times 10^6 M_\odot$ (Solomon et al. 1987), roughly consistent with the Toomre mass. In the Milky Way, and possibly in other galaxies, molecular clouds are surrounded by atomic gas with a similar or slightly smaller mass.

The clouds appear to be somewhat centrally concentrated. We will often employ a Larson-law density distribution,

$$\rho(r) \sim r^{-1}, \quad (3)$$

where r is the distance from the center of the GMC. We also explored isothermal models $\rho(r) \sim 1/r^2$; we find that such clouds are slightly easier to disrupt than the less centrally concentrated Larson-law clouds in the optically thick limit.

2.2.1. But are there molecular clouds in ULIRGs?

GMCs are observed in the Milky Way, and in nearby star-forming galaxies such as M82. We see clumps of gas in “chain” or “clump” star-forming galaxies at $z = 2$, such as Q2346-BX 482 discussed below. These have been interpreted as self-gravitating, i.e., as GMCs (e.g., Genzel et al. 2008). However, we do not know of any direct evidence for Toomre mass self-gravitating objects in ULIRGs. There is some evidence against such objects: since the clouds are self-gravitating, they will have a slightly higher velocity dispersion than that of the disk out of which they form. Increasing the velocity dispersion will alter the inferred gas mass (see Downes & Solomon 1998). Putting too much gas in gravitationally bound objects will increase the apparent gas mass, possibly making it larger than the dynamical mass.

One the other hand, ongoing star formation is clearly seen in Arp 220. Star formation probably requires densities exceeding 10^6 cm^{-3} to proceed. Thus there is evidence that *some* gas is gravitationally bound. Moreover, there are numerous massive compact star clusters observed in Arp 220 (Wilson et al. 2006), indicating that massive, bound, and relatively compact accumulations of gas existed in the recent past. Motivated by these considerations, we will assume that Toomre-mass self-gravitating objects exist in all star-forming galaxies, including ULIRGs.

2.3. Gas clump and stellar cluster mass distributions

Most of the gas in Milky Way GMCs is diffuse ($n \lesssim 3 \times 10^2 \text{ cm}^{-3}$), but a fraction of order 10% is in the form of dense gas clumps, with sizes around 1 pc (Lada & Lada 2003) and masses from a few tens to a few thousand solar masses. The clumps have a mass distribution similar to that for clouds (eq. 2), with an exponent $\alpha_c \approx 1.7$ (Lada & Lada 2003).

TABLE 1
OBSERVED GALAXY PARAMETERS

Galaxy	R_d kpc	t_{dyn} yr	Σ g cm $^{-2}$	v_T km s $^{-1}$	Z/Z_\odot	\dot{M}_* (obs) M_\odot yr $^{-1}$
Milky Way	8.0	3.6×10^7	2×10^{-3}	6	1	2.0
M82	0.35	3.0×10^6	0.1	15	1.5	4
BX482	7.0	2.9×10^7	4×10^{-2}	53	1	140
Arp 220	0.1	3.3×10^5	7	61	3	120

NOTE. — Observed galaxy properties. Column one gives the name of the model. The next five columns give model input parameters: the disk radius (col. 2), dynamical time R_d/v_c (col. 3), gas surface density (col. 4), turbulent velocity v_T (col. 5; recall that $H = [v_T/v_c]R_d$), and metallicity in solar units (col. 6). The metallicity is not that well-constrained in Arp 220. Column 7 gives the observed star formation rate for the galaxies.

In both the Milky Way (Elmegreen & Efremov 1997; van den Bergh & Lafontaine 1984) and in nearby galaxies (McKee & Williams 1997; Kennicutt et al. 1989), the number of stellar clusters of mass m_* is given by

$$\frac{dN_{*cl}}{dm_{*cl}} = N_{*cl,0} \left(\frac{m_{*cl,0}}{m_{*cl}} \right)^{\alpha_{cl}} \quad (4)$$

with $\alpha_{cl} \approx 1.8$. In other words, most stars form in massive clusters; in the Milky Way, at least, these clusters are made from gas in massive gas clumps, inside of massive GMCs.

2.4. The Sizes of Star Clusters

Star clusters are observed to have sizes ranging from $r_{cl} \approx 0.1$ pc (for $M_{cl} \approx 10M_\odot$) to $r_{cl} \approx 10$ pc ($M_{cl} \approx 10^8M_\odot$). There are hints that clusters with masses $M_{cl} \lesssim 10^4M_\odot$ have a mass-radius relation of the form

$$r_{cl} \approx 2 \left(\frac{M_{cl}}{m_0} \right)^\beta \text{ pc} \quad (5)$$

with $m_0 = 10^4M_\odot$ and $\beta \approx 0.4$ (Lada & Lada 2003), but it is entirely possible that this is a selection effect. Intermediate mass clusters, those with $10^4M_\odot \lesssim M_{cl} \lesssim 3 \times 10^6M_\odot$ have $r_{cl} \simeq 2$ pc independent of mass ($\beta = 0$), albeit with substantial scatter. This characteristic size is seen for young ($\lesssim 30$ Myr) and old ($\gtrsim 30$ Myr) clusters in M51 with masses in the range $10^3 - 10^6M_\odot$ (Scheepmaker et al. 2007), for super star clusters in M82 with $M_{cl} = 10^5 - 4 \times 10^6M_\odot$ (McCradly et al. 2003; McCradly & Graham 2007), and in globular clusters with masses $\sim 10^5 - 10^6M_\odot$ (Harris 1996). Finally, high-mass clusters with $M_{cl} \gtrsim 10^6M_\odot$ have $\beta = 0.6$ and $m_0 = 10^6M_\odot$ in equation (5) (Walcher et al. 2005; Evstigneeva et al. 2007; Barmby et al. 2007; Rejkuba et al. 2007; Murray 2009). When using the radii of stellar clusters in our GMC models, we will be guided by these observed mass-radius relations.

3. A MODEL OF CLUSTER & GMC DISRUPTION

We start by specifying the properties of the disk in which the GMC lives; the effective disk radius R_d , the circular velocity v_c , the disk scale height H_d , the disk gas mass M_d and metallicity Z/Z_\odot (relative to solar). We choose the values of these parameters to match those of four galaxies to which we compare our models: the Milky Way, M82, Q2346-BX 482,

TABLE 2
GMC AND STAR CLUSTER PROPERTIES

Galaxy	R_{GMC} pc	M_{GMC} M_\odot	r_{cl} pc	M_* M_\odot	ϵ_{GMC}	v_T km s $^{-1}$
Milky Way	100	3×10^6	2	10^5	0.03	5
M82	23	3×10^6	1.5	7×10^5	0.24	10
BX482	925	10^9	13	2.7×10^8	0.27	50
Arp 220	5	4×10^7	3.5	1.4×10^7	0.38	50

NOTE. — Columns 2-5 give the assumed GMC and star cluster properties: the radius of the GMC R_{GMC} (col. 2), the mass of the GMC M_{GMC} (col. 3), the star cluster radius r_{cl} (col. 4), and the stellar mass of the star cluster M_* (col. 5). Columns 6 and 7 give the predictions of our model for the star formation efficiency in the GMC ϵ_{GMC} and the shell velocity when the GMC is disrupted, which we also interpret as the turbulent velocity v_T induced in the ISM of the Galaxy.

and Arp 220. In that sense these are not free parameters. Table 1 summarizes the observed input parameters for the galactic disks in the systems we model, while Table 2 gives the inferred or assumed input parameters related to the GMC and its central star cluster: the mass M_{GMC} and radius R_{GMC} of the GMCs and the stellar mass and radius of the star clusters. Table 2 also lists the GMC's star formation efficiency ϵ_{GMC} and the shell velocity when the GMC is disrupted – we interpret the latter as the turbulent velocity induced in the ISM, v_T .

We employ a one-dimensional model for the GMC, with the free parameter $\phi_G \equiv H_d/R_{\text{GMC}}$ defining the size of a GMC with respect to the disk in which it resides. In the Milky Way this ratio is about $\sim 2-5$ for the most massive clouds; for specific cases like G298.4-0.3, which has $R_{\text{GMC}} \approx 100$ pc, we use the observed ratio. In models for other galaxies we fix $\phi_G = 4$. The mass of the GMC is taken to be the Toomre mass, with a Larson-like ($\rho \sim 1/r$) internal density profile.

For the purposes of our simplified modeling, the stars are assumed to lie in a single massive cluster of total mass (gas plus stars) M_{cl} , which forms a mass of stars $M_* = \epsilon_{cl}M_{cl}$ with luminosity L , surrounded by the remnants of the gas out of which it formed, with mass $M_g = (1 - \epsilon_{cl})M_{cl}$. We use a Muench et al. (2002) stellar initial mass function (IMF) to relate the cluster luminosity to its mass. The quantity ϵ_{cl} characterizes the efficiency with which cluster gas is turned into stars. In our galaxy $\epsilon_{cl} \approx 0.3-0.5$ (Lada & Lada 2003). In our models, we fix $\epsilon_{cl} \simeq 0.5$ and adjust the cluster mass M_{cl} (or equivalently, the cluster stellar mass M_*) to find under what conditions the central star cluster can disrupt its host GMC. Physically, we expect that star formation will self-adjust to a form a cluster of approximately this mass. For the Milky Way and M82 the star cluster masses we infer by this method are comparable to those observed.

We model the impact of the central star cluster on the surrounding GMC using the thin shell approximation. As the star cluster evolves, driving winds, jets, and radiation into the overlying shell of gas, we calculate the shell's dynamics as it sweeps up mass and disrupts the GMC. The relation between shell radius r , shell velocity $v(r)$, shell mass $M(r)$, and shell momentum $P_{sh}(r)$ is given by

$$\frac{dr}{dt} = \frac{P_{sh}}{M(r)}, \quad (6)$$

where $M(r)$ is the mass of the shell, which increases as the shell radius r increases, and $P_{sh} = M(r)v(r)$ is the momentum

of the shell. For a Larson-like density profile of the GMC, $\rho \propto r^{-1}$, the mass of the shell is given by

$$M(r) = (1 - \epsilon_{\text{cl}})M_{\text{cl}} + M_{\text{GMC}} \left[\left(\frac{r}{R_{\text{GMC}}} \right)^2 - \left(\frac{r_{\text{cl}}}{R_{\text{GMC}}} \right)^2 \right] \quad (7)$$

for $r < R_{\text{GMC}}$ and by

$$M(r) = (1 - \epsilon_{\text{cl}})M_{\text{cl}} + M_{\text{GMC}} + \frac{4\pi}{3}(r^3 - R_{\text{GMC}}^3)\rho_{\text{disk}} \quad (8)$$

for $R_{\text{GMC}} < r < H$. We have experimented with both isothermal ($M_{\text{GMC}}(r) \sim r$) and Larson ($M_{\text{GMC}}(r) \sim r^2$) GMCs and find qualitatively similar results.

The momentum equation for the shell is

$$\frac{dP_{\text{sh}}}{dt} = -F_{\text{grav}} - F_{\text{ram}} - F_{\text{turb}} + F_{\text{HII}} + F_{\text{rad}} + F_{\text{jet}} + F_{\text{hot}} + F_{\text{cr}} \quad (9)$$

The inward forces on the right-hand side of equation (9) are the self gravity F_{grav} of the swept up shell and the mutual gravity of the stars in the largest cluster and the shell, the force F_{turb} exerted by the turbulent motions of the gas in the GMC on the shell, and the force F_{ram} produced by ram pressure as the shell sweeps up the material of the GMC or the surrounding gas disk. The outward forces on the right-hand side of equation (9) acting to disrupt the GMC include the force F_{jet} associated with momentum deposited by jets from star formation, the force F_{HII} due to the thermal pressure from ionized gas (HII regions) and from shocked stellar winds, and the force F_{rad} associated with radiation pressure. In some models we include the effects of hot gas F_{hot} and cosmic rays F_{cr} associated with shocked stellar wind. A more detailed description of how we implement these forces is given in Appendix A.

We assume that stellar wind energized hot gas ($\sim 10^7$ K) does not play a dynamical role in galaxies like the Milky Way; we show explicitly in this paper that even in the most optimistic cases such winds are not important for GMC disruption in ULIRGs. Much of the literature on bubbles around massive stars and massive star clusters assumes that shocked stellar winds dominate the dynamics (e.g., Castor et al. 1975; Weaver et al. 1977; Chu & Mac Low 1990). However, observations of HII regions in the Milky Way suggest that the pressure in such hot gas is equal to that of the associated HII (10^4 K) gas (Dorland & Montmerle 1987; McKee, Van Buren, & Lazareff 1984; Harper-Clark & Murray 2009). The most likely interpretation of these results is that neither hot gas nor cosmic rays are confined inside bubbles in the Milky Way or the LMC, but rather escape (Harper-Clark & Murray 2009). Accordingly, we neglect the last two terms on the right hand side of equation (9) in our Milky Way models and in our M82 models; calculations which include these pressures predict bubble sizes that are far too large compared to observations in the Milky Way. Accordingly, with the exception of §4.4, we ignore the pressure associated with shocked stellar winds. We do include stellar-wind and cosmic-ray pressure in our Arp 220 models, but there they make little difference.

In §1, we made a distinction between feedback in the disk as a whole, and feedback in GMCs. This distinction is important for a number of reasons. In particular, we believe that supernova (SN) explosions largely contribute to the former, but not the latter. In $z \sim 0$ ULIRGs, where the bulk of the star formation takes place in ~ 100 pc disks, the dynamical

time is $t_{\text{dyn}} = R/v_c \approx 5 \times 10^5$ yr, much less than the main sequence lifetime of even the most massive stars. Hence a gravitationally bound object in a ULIRG cannot be disrupted on a dynamical time by SNe resulting from stars formed in that object. In the Milky Way, even though the dynamical time is longer than the main sequence lifetime of massive stars, it is clear that GMCs are in the process of being disrupted well before SNe occur (Murray & Rahman 2009). Although SNe may be important during late stages of GMC disruption, and for stirring up the galactic disk as a whole, they cannot be the main agent that disrupts GMCs, either in Milky Way-like galaxies or in ULIRGs. For this reason, we do not include the force due to SNe in equation (9).

In the densest starbursts, which have mean gas densities $\sim 10^{3-4} \text{ cm}^{-3}$, SNe rapidly lose the majority of their energy to radiative losses (e.g., Thornton et al. 1998). Under these conditions, the primary role of SNe is to stir up the bulk of the ISM via the momentum they supply, rather than to heat up the gas and/or create a hot phase of the ISM in pressure equilibrium with the rest of the mass (Thompson et al. 2005). To see that the latter is untenable, we estimate the density n_h of hot gas required for a virialized ISM at $\sim 10^7 T_7$ K to be in pressure equilibrium with the bulk of the gas, i.e., for $p_h = n_h kT \simeq \pi G \Sigma_g^2$. Given this density, we find that there is a critical surface density Σ_c above which thermal X-ray emission from the hot gas would exceed the observed correlation between X-ray and FIR emission ($L_X \simeq 10^{-4} L_{\text{FIR}}$; Ranalli et al. 2003): $\Sigma_c \simeq 0.04 (H_d/100 \text{ pc})^{-2/5} T_7^{3/5}$. Galaxies with $\Sigma_d \gtrsim \Sigma_c$, which includes the majority of luminous star-forming galaxies, cannot have a dynamically important hot ISM. Instead, the dominant role of SNe is to stir up the dense gas via the momentum imparted in the snowplow phase. This may even be true in galaxies with $\Sigma_c \lesssim \Sigma_d$, because the hot gas can vent via galactic winds or fountains. For example, in the Milky Way, which has $\Sigma_d \simeq 2.5 \times 10^{-3} \text{ g cm}^{-2} \ll \Sigma_c$, the hot ISM is believed to contribute only $\sim 10\%$ of the total pressure (Boulares & Cox 1990). For this reason, we will not consider the pressure due to the hot ISM in this paper, although the momentum supplied by SNe is important in the late stages of star cluster and GMC evolution.

Having summarized the basic elements of our model, we now describe its application to galaxies ranging from the Milky Way to the most luminous starbursts (§4). We then discuss the implications of these results (§5).

4. RESULTS

4.1. The Milky Way: G298.4-0.3

Recent work has revealed that the Milky Way harbors a number of very young massive star clusters, with masses ranging up to $10^5 M_\odot$ (Figer et al. 1999; Brandner et al. 2008; Figer et al. 2006; Murray & Rahman 2009). We examine the case of G298.4-0.3 in the Carina arm. Murray & Rahman (2009) show that the free-free flux emerging from this region implies a total ionizing flux $Q = 7.7 \times 10^{51} \text{ s}^{-1}$, and suggest that $\sim 60\%$ of this comes from a single massive cluster residing in the prominent ~ 50 pc bubble revealed by Spitzer GLIMPSE images. Most of the remaining flux comes from two clusters associated with the two giant HII regions G298.2-0.3 and G298.9-0.4; both sources appear to lie in the rim of the bubble seen in the GLIMPSE images. Grabelsky et al. (1988) find two massive GMCs in this region, numbers 24 and 26,

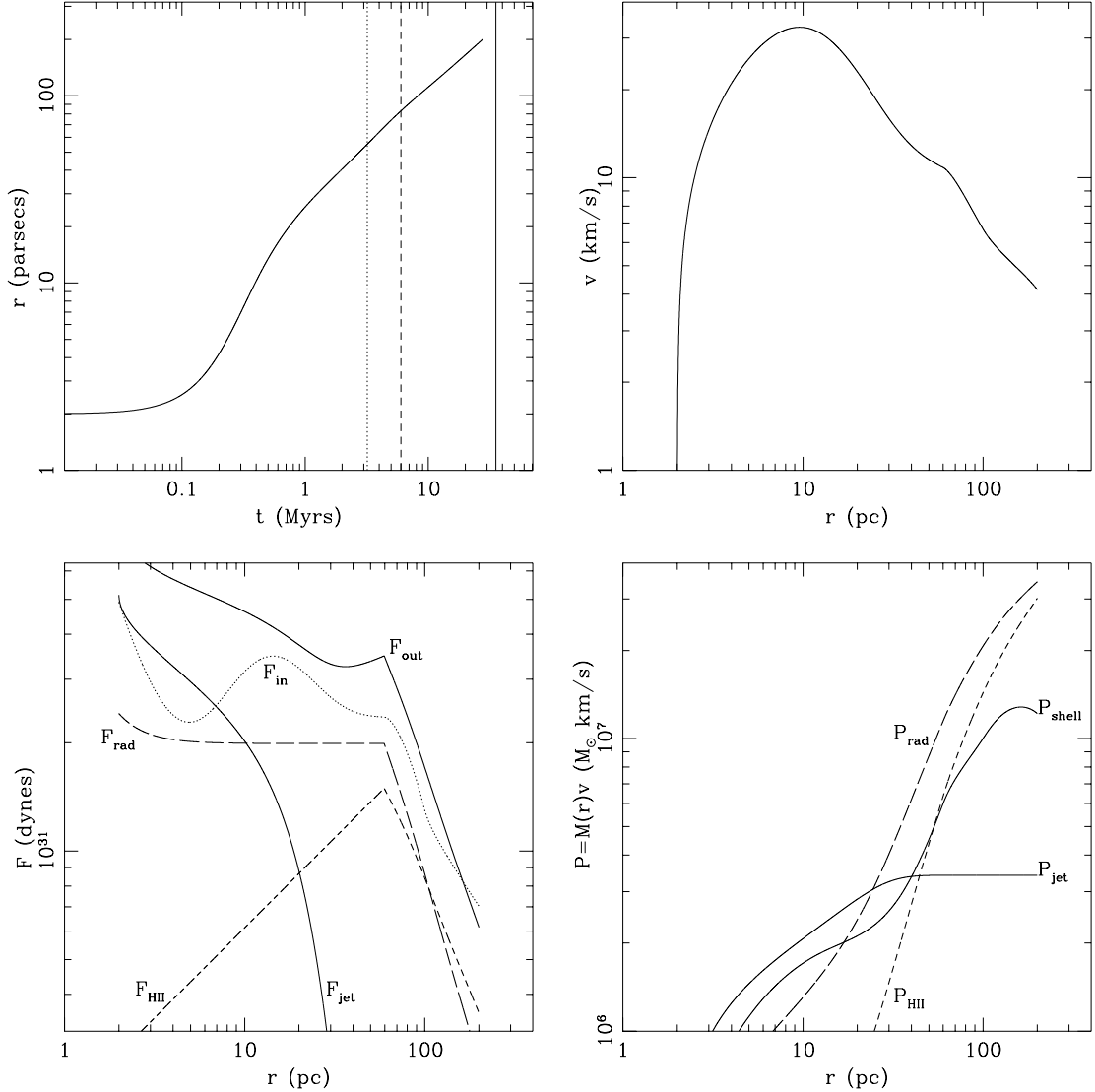


FIG. 1.— Shell radius as a function of time and velocity, forces, and shell momentum as a function of radius in our model for G298.4-0.3 in the Milky Way. The shell is sheared apart when it reaches the Hill radius (~ 200 pc), where we end our integration. *Upper left*: The dotted, dashed, and solid lines mark when the first cluster SNe explode, the central cluster luminosity drops to 1/3 of its initial value, and t reaches the Milky Way dynamical timescale, respectively. *Upper right*: The velocity of the swept-up shell in G298.4-0.3 as a function of shell radius. Note that the asymptotic velocity is comparable to the turbulent velocity of the Milky Way disk. *Lower left*: The upper-most solid line is the total outward force, consisting of the momentum supplied by protostellar jets (solid line; F_{jet}), by HII gas pressure (short dashed line; F_{HII}) and radiation pressure on dust grains (long dash line; F_{rad}). The dotted line is the total inward force (F_{in}), dominated by the self-gravity of the shell. *Lower right*: Momentum of the swept-up shell in G298.4-0.3 (solid line), together with the momentum deposited by radiation (long dashed line), gas pressure (short dashed line), and protostellar jets (solid line, labeled P_{jet}). The bulk of the momentum is supplied by radiation and gas pressure, but the early contribution of the protostellar jets is important in the disruption of the natal cluster gas.

both with $M_{\text{GMC}} \approx 3 \times 10^6 M_{\odot}$ and $R_{\text{GMC}} \approx 100$ pc. Their radial velocities are 22 km s^{-1} and 24 km s^{-1} , in good agreement with the range of radio recombination line, i.e., HII region, radial velocities in this direction, which range from $+16 \text{ km s}^{-1}$ to 30.3 km s^{-1} , with a mean $\sim +23 \text{ km s}^{-1}$.

Accordingly, our model for G298.4-0.3 consists of a GMC with $R_{\text{GMC}} = 100$ pc and $M_{\text{GMC}} = 3 \times 10^6 M_{\odot}$. In the spirit of our simplified one-dimensional modeling, we lump all of the star clusters together into a central star cluster with $L \approx 7 \times 10^7 L_{\odot}$ and initial cluster radius $r_{\text{cl}} = 1.5$ pc. Half the Galactic star formation takes place in 17 star clusters, with a minimum $Q = 3 \times 10^{51}$, so G298.4-0.3 is representative of star forming clusters in the Milky Way.

The top two panels of Figure 1 show the radius of the shell surrounding the central cluster as a function of time and the shell velocity as a function of radius. The shell starts at our putative initial radius for the cluster of ~ 1.5 pc, and reaches $r \sim 80$ pc at about 6.5 Myr (dashed line), at which point the star cluster luminosity has dropped by a factor of 3. The most massive stars begin to explode after about 3.6 Myr (vertical dotted line), while the last O stars explode after about 1.3×10^7 yr. The solid vertical line marks the dynamical time R/v_c for the Milky Way at $R = 8$ kpc. Note that the dynamical time for the GMC is somewhat shorter, ~ 6 Myr.

The lower left panel of Figure 1 shows the forces as a function of radius in this model; note that the radiation and HII gas pressures drop after 6.5 Myrs, when the bubble has $r \sim 100$

pc, but the bubble continues to expand at the same rate. The evolution after 6.5 Myrs, i.e., radii larger than ~ 50 pc, may underestimate the rate of expansion somewhat; the bubble may expand slightly more rapidly after several Myrs due to energy input by SNe. We say the rate of expansion *may* be underestimated since the hot gas from the SNe is likely to escape the bubble as easily as the hot gas from shocked winds apparently does. In addition to SNe, other unmodeled effects also become important at late times and large radii. For example, because the inner radius of the shell exceeds the outer radius of the initial GMC, the surface density of the gas decreases to $A_V \approx 1$, so that ionizing photons from the Galactic radiation field can penetrate and ionize the shell.

We halt the integration in our model when the radius of the expanding bubble exceeds the Hill radius r_{Hill} of the GMC, i.e., when the tidal shear from the Galaxy exceeds the self-gravity of the GMC: $r_{\text{Hill}} \approx (M_{\text{GMC}}/2M(r))^{1/3}a$, where $M(r) = v_c^2 a / G$ is the enclosed dynamical mass of the galaxy at the galactocentric radius a of the GMC. After this time the remaining molecular gas will be dispersed (although not necessarily converted to atomic gas).

Figure 1 shows that the central cluster in G298.4-0.3 should disrupt its natal GMC. What force is responsible for this disruption? At the current radius, ~ 55 pc, the radiation force and the gas pressure force are within a factor of two of each other, and will remain so until most of the O stars explode; the force from protostellar jets is substantially smaller. However, at early times, the jet force was as much as a factor of two larger than the radiation pressure force, and the gas pressure force was negligible.

Finally, the lower right panel of Figure 1 plots the momentum of the shell as a function of time. At the current radius of the bubble in G298.4-0.3, $r \sim 55$ pc, the radiation has deposited about twice the momentum supplied by the HII gas pressure. The stellar jets are not active at this time, but over the time they were active (corresponding to radii below ~ 15 pc) they deposited a momentum comparable to that of the radiation pressure (at those early times). In these models, a combination of proto-stellar jets and radiation pressure disrupts the natal cluster, while a combination of gas and radiation pressure disrupts the GMC. The shell velocity at late times is of the order of the turbulent velocity seen in the ISM of the Galaxy (upper right panel), demonstrating that, even in the absence of supernovae, massive star formation can generate turbulent motions on large (50 pc or larger) scales comparable to those observed.

4.2. The Starburst M82

M82 is one of the nearest ($D = 3.6$ Mpc; Freedman et al. 1994) starburst galaxies, with an infrared luminosity $L_{\text{IR}} = 5.8 \times 10^{10} L_{\odot}$ (Sanders et al. 2003). The galaxy is small compared to the Milky Way, with a circular velocity $v_c \approx 110 \text{ km s}^{-1}$ (Young & Scoville 1984), and a CO inferred gas mass $2 \times 10^8 M_{\odot}$ inside $r = 350$ pc (Weiß et al. 2001) (adjusted to our assumed distance), yielding a gas surface density $\Sigma_g \approx 0.1 \text{ g cm}^{-2}$ and a gas fraction $f_g \approx 0.2$. The metallicity is 1.2–2.0 times solar (Smith et al. 2006).

The radius and mass of the most massive star clusters in M82 are well established; there are about 200 clusters with $M > 10^4 M_{\odot}$ (Melo et al. 2005) and about ~ 20 well studied super star clusters ($M_{\text{cl}} > 10^5 M_{\odot}$). With one arcsec-

ond corresponding to a spatial scale of 17.5 pc, a number of super star clusters are resolved by HST (Smith & Gallagher 2001; McCrady et al. 2003; McCrady & Graham 2007). Typical half light projected radii for these massive objects are $\sim 0.08''$ or 1.4 pc. McCrady et al. (2003) list 20 such clusters. The total mass of the 15 clusters for which they measure viral masses is $\sim 1.4 \times 10^7 M_{\odot}$. Their largest cluster, ‘L’, is a monster, with a mass of $4 \times 10^6 M_{\odot}$ and a half-light radius of 1.5 pc; more typical masses are $\sim 5 \times 10^5 M_{\odot}$. A rough fit of the form (4) gives $\alpha_{\text{cl}} \approx 1.9$ (McCrady & Graham 2007).

The masses of the GMCs in M82 are also known; the distribution is well fitted by equation (2), with $\alpha_G \approx 1.5 \pm 0.1$, and a maximum mass of $M_{\text{GMC}} \approx 3 \times 10^6 M_{\odot}$ (Keto et al. 2005). The Toomre mass is $\approx 7 \times 10^6 M_{\odot}$. Both are comparable to the mass of the two largest super star clusters given by McCrady & Graham (2007). Either there were more massive GMCs in M82 in the past, or $\epsilon_{\text{GMC}} \approx 1$ for the GMCs out of which these two clusters formed.

Tables 1 & 2 summarize our assumed galaxy, GMC, and star cluster properties in M82. These are all motivated by, and reasonably consistent with, the observations summarized above. Our results for the disruption of GMCs are summarized in Figure 2. The top two panels show the shell radius as a function of time and the velocity as a function of radius. The main sequence lifetime of a $120 M_{\odot}$ star (the dashed vertical line) is comparable to the disk dynamical time (R_d/v_c , the solid vertical line). The GMC is disrupted (reaches the Hill radius) about one disk dynamical time after the cluster forms. The velocity of the shell reaches higher values than those found in our Milky Way model because of the much larger cluster masses in M82, combined with the fact that the star cluster radii in the two galaxies are nearly the same. Initially, the shell velocity is comparable to the escape velocity from the cluster. The velocity begins to slow once the swept up mass is similar to the mass in the cluster (at $r \sim 4$ pc).

What is responsible for disrupting the GMC in our M82 model? The lower panels of Figure 2 show that the cluster gas on small scales is expelled by a combination of protostellar jets and radiation pressure, while the overlying GMC is disrupted primarily by radiation pressure. The contribution from the gas pressure of the HII region is negligible over most of the evolution: the lower right panel shows that the H II gas pressure contribution to the momentum is $\sim 10\%$ of that contributed by radiation when the shell radius reaches the original size of the GMC.

4.3. The Clump Galaxy Q2346-BX 482

Q2346-BX 482 is a redshift $z = 2.26$ disk galaxy with a disk radius of $R_d \approx 7$ kpc and a gas mass, as estimated from inverting the Schmidt Law in Kennicutt (1998), of $M_g \approx 3 \times 10^{10} M_{\odot}$ (Genzel et al. 2008). We interpret the clumps in rapidly star forming redshift $z \sim 2$ galaxies as Toomre mass GMCs, with radii $R_{\text{GMC}} \approx 1$ kpc, and we model the giant clump in BX 482, as one of the most extreme examples of this phenomenon. With turbulent and circular velocities of $v_T \approx 55 \text{ km s}^{-1}$ and $v_c \approx 235 \text{ km s}^{-1}$, respectively, we infer a disk scale height of $H \approx 1.6$ kpc, and using $\phi_G = 3$ a GMC size of order 500 pc. For comparison, the observed clumps are modestly larger than this, around 1 kpc.

The mass of the central star cluster is set so that the luminosity matches that observed, roughly $L \approx 4 \times 10^{11} L_{\odot}$ (Gen-

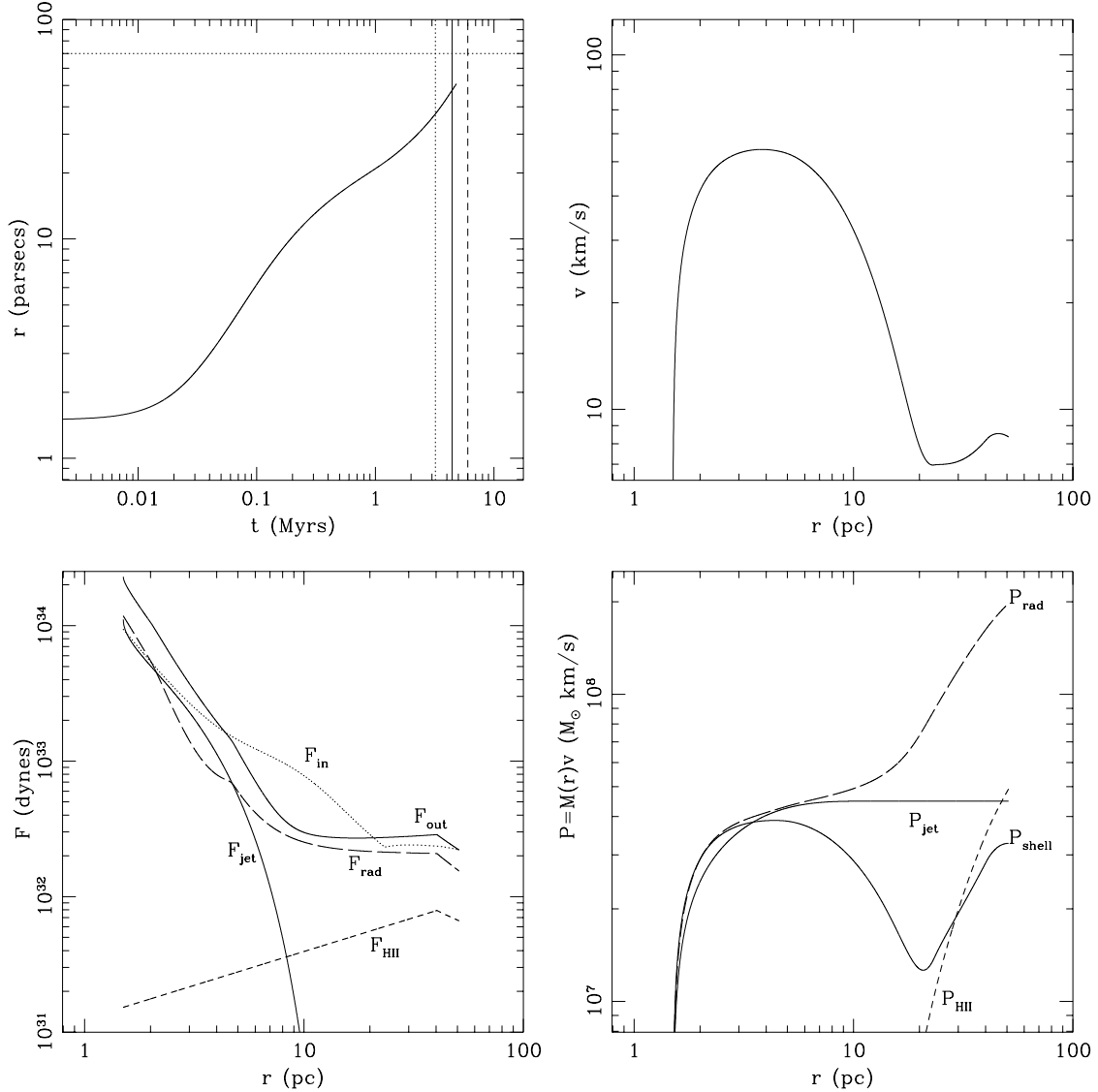


FIG. 2.— Shell radius as a function of time and velocity, forces, and shell momentum as a function of radius in our model for the disruption of a GMC by a massive star cluster in the starburst M82. *Upper left*: Bubble radius as a function of time. The dashed line is when the star cluster luminosity drops to 1/3 of its initial value, while the dotted vertical line marks the lifetime of a $120M_{\odot}$ star. The shell is disrupted by ambient differential rotation and tidal forces in the galaxy at the Hill radius (solid line); this occurs roughly when the first supernovae explode. *Upper right*: The velocity of the swept-up shell in the M82 model as a function of shell radius. *Lower left*: The forces in our M82 model, plotted against the radius of the swept up shell. Line styles are the same as in Figure 1. *Lower right*: The momentum of the swept-up shell in the M82 model, with the same line styles as in Figure 1. The bulk of the momentum is supplied by radiation; the contribution from gas pressure is negligible. The early contribution of the protostellar jets is important in the disruption of the natal cluster gas.

zel, private communication). We take the radius of the star cluster to be ~ 7 pc (see §2.4). In reality, there will likely be many star clusters, with a distribution given by equation 4, and with a spread in age of several to ten Myrs. We assume solar metallicity, consistent with the observations. Finally, the gas mass of the clump is not known, but we assume it is roughly the Toomre mass, $\sim 10^9 M_{\odot}$. This is consistent with the mass of ionized gas for the observed luminosity of the clump, at the observed size $R_{\text{GMC}} \approx 1$ kpc, and for a stellar population less than 4 Myrs old (eqs. A10 & A12).

Figure 3 shows the results of our model for the giant GMC in Q2346-BX 482. The right panel shows that radiation pressure dominates the evolution of the GMC at nearly all times. The GMC is disrupted in about 15 Myrs, half the disk dynamical time scale. The shell velocity, shown in the middle panel,

is $\sim 30-80 \text{ km s}^{-1}$ when the radius is $0.5-1$ kpc, in reasonable agreement with the observed velocity dispersion of the galaxy. Note that the decrease in velocity at late times (due to the decrease in radiation pressure seen in the right panel) is probably not that physical given that the shell is in the process of being sheared apart by the rotation of the galaxy.

Our conclusion that radiation pressure is disrupting the massive clump in BX482 is directly supported by observations, independent of the specific assumptions in our model: the self-gravity of the clump is

$$F_{\text{grav}} = \frac{GMM}{2r^2} = 3 \times 10^{34} \left(\frac{M}{10^9 M_{\odot}} \right)^2 \left(\frac{1 \text{ kpc}}{R_{\text{GMC}}} \right)^2 \text{ dynes}, \quad (10)$$

where we have scaled M to the Toomre mass. This can be

compared directly with the radiation pressure force,

$$F_{\text{rad}} = \frac{L}{c} = 5 \times 10^{34} \left(\frac{L}{4 \times 10^{11} L_{\odot}} \right) \text{ dynes.} \quad (11)$$

The clump should thus be expanding.

4.4. The Ultra-Luminous Infrared Galaxy Arp 220

Arp 220, at ~ 77 Mpc, is the proto-typical ULIRG in the local universe. The gas mass of each of the $r_d \approx 100$ pc star-forming disks in Arp 220 is $10^9 M_{\odot}$, the circular velocity $v_c \approx 300 \text{ km s}^{-1}$, $v_T \approx 80 \text{ km s}^{-1}$, and the disk scale height $H = (v_T/v_c)r_d \approx 23$ pc (Downes & Solomon 1998; Sakamoto et al. 1999). The mean surface density is $\Sigma_g \approx 7 \text{ g cm}^{-2}$, about 100 times larger than that of M82 and more than a thousand times higher than in the Milky Way. We estimate that Arp 220 has GMC masses of $\approx 5 \times 10^7 M_{\odot}$, $R_{\text{GMC}} \approx 5$ pc and a turbulent velocity in each GMC of $\sim 170 \text{ km s}^{-1}$, about twice that measured for the disk as a whole. Although the metallicity is uncertain, we take a fiducial metallicity of 3 times solar; this increase in metallicity is important because it increases the dust optical depth and hence the overall importance of radiation pressure.

Wilson et al. (2006) found ~ 40 young superstar clusters in and around Arp 220; they estimate masses for about a dozen, with a number having $M_{\text{cl}} \sim 2-4 \times 10^6 M_{\odot}$; the largest has $M_{\text{cl}} \approx 10^7 M_{\odot}$. Given the huge extinction toward the twin disks, this is likely to be a rather conservative lower limit on the mass of the most massive cluster in the system. The clusters are unresolved in the HST images (which have a resolution of order 15 pc at the distance of Arp 220), except possibly their brightest cluster, with a half light radius $r_{\text{cl}} \approx 20$ pc. Wilson et al. (2006) do not obtain either a velocity dispersion or a half light radius for their clusters, so they cannot calculate a dynamical mass. Rather, they use a Salpeter IMF and Bruzual & Charlot (1993) stellar synthesis models combined with their photometry.

We find that for $M_{\text{cl}} = 1.4 \times 10^7 M_{\odot}$ ($L = 3 \times 10^{10} L_{\odot}$), even a Toomre mass GMC ($4 \times 10^7 M_{\odot}$) in Arp 220 would be disrupted (see Fig. 4). The disruption of the GMC occurs on the dynamical time of the disk, well before any supernovae explode in the GMC's central star clusters.

Our estimated GMC mass in Arp 220 ($5 \times 10^7 M_{\odot}$) is a factor ten higher than the largest GMC mass seen in M82; this is a result of the much larger surface density in Arp 220 compared to M82. In contrast, the star cluster masses found so far in Arp 220 are only a factor 2–3 times larger than the masses of the largest clusters observed in M82, the latter being around $2-4 \times 10^6 M_{\odot}$ (McCraday & Graham 2007). Given that our predicted GMC star formation efficiency is not that different in the two cases (Table 2), we expect that more massive clusters are lurking in Arp 220.

The right panel of Figure 4 shows the forces acting on the shell of swept up mass in our model of Arp 220. As in Figures 1 and 2, the force due to proto-stellar jets is initially similar to that due to radiation pressure. This situation lasts only while the shell accelerates from the initial clump radius of about 4 pc, until the shell reaches a little less than 6 pc. For the rest of the evolution radiation pressure provides the only significant outward force. The outward force supplied by ionized gas is completely negligible; the short dash line in the Figure

is the gas pressure *multiplied by 100*. Both the hot gas and cosmic rays produced by shocked stellar winds are dynamically unimportant, even though we have assumed complete trapping of the shocked stellar wind material (an assumption that fails in the Milky Way; Harper-Clark & Murray 2009).

The middle panel of Figure 4 shows that radiation pressure will stir the ISM of Arp 220 to $\sim 50 \text{ km s}^{-1}$, somewhat less than the escape velocity from the cluster and similar to the velocity dispersion seen in CO observations.

5. DISCUSSION

5.1. The Importance of Radiation Pressure

Using four examples that cover conditions ranging from Milky Way-like spirals to the densest starbursts (see Tables 1 & 2), we have explored the physical processes that can disrupt giant molecular clouds (GMCs), one of the basic building blocks of star formation. We find that radiation pressure produced by the absorption and scattering of starlight by dust grains can contribute significantly to disrupting GMCs in nearly all types of galaxies. By contrast, protostellar jets are important only at early times during GMC disruption while the thermal gas pressure in HII regions is important for GMC dispersal in spiral galaxies like the Milky Way, but not in more luminous starbursts. For the Milky Way and M82, where the observations are particularly detailed, our results demonstrate that observed massive star clusters have precisely the luminosities and structural properties required to disrupt Toomre-mass GMCs via radiation pressure.

The results presented here support Thompson et al. (2005)'s model of radiation pressure supported star-forming galaxies. In that paper, we focused on the large-scale properties of star formation in galaxies and the fueling of massive black holes in galactic nuclei. Here we have extended that model by taking into account the fact that star formation is not smooth and homogeneous; rather, most stars form in massive star clusters inside massive GMCs (§2). Our conclusion that Toomre-mass GMCs can be disrupted by radiation pressure is qualitatively and quantitatively similar to Thompson et al.'s conclusion that radiation pressure can regulate star formation in galactic disks to have Toomre's $Q \approx 1$.

It is useful to consider simple scaling arguments in order to understand why, over the range of surface densities probed by the observed Schmidt Law ($10^{-3} \text{ g cm}^{-2} \lesssim \Sigma_g \lesssim 10 \text{ g cm}^{-2}$), radiation pressure is the most viable mechanism for GMC disruption. To rough approximation, the self-gravity of the gas in a GMC is

$$F_{\text{sh}} = \phi_G^2 \frac{GM_T M_T}{2H^2} \propto \frac{M_T^2}{H^2} \propto M_T \Sigma_g, \quad (12)$$

which varies by a more than a factor of $\sim 10^6$ from normal galaxies to starbursts.

We can compare this force directly to the radiation pressure force. In the optically thin limit⁸

$$F_{\text{rad}} = \frac{L}{c} = \frac{\Psi M_*}{c}, \quad (13)$$

⁸ By this we mean that the GMC is optically-thick to the UV, but optically-thin to the re-radiated FIR emission.

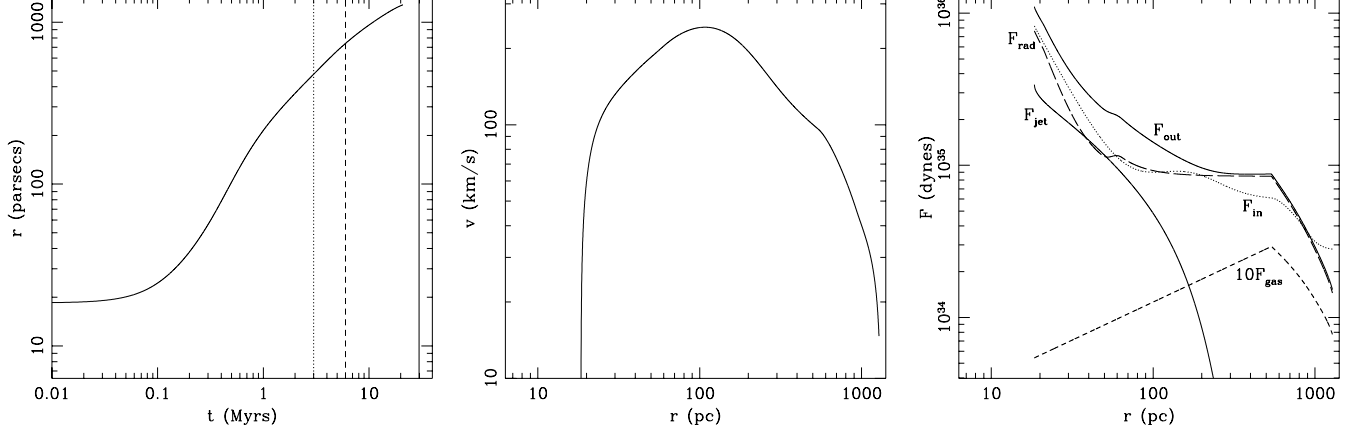


FIG. 3.— *Left*: The radius of the shell as a function of time in the model for the giant clump in the $z = 2.26$ galaxy Q2346-BX 482. The dotted, dashed, and solid lines mark when the first cluster SNe explode, the central cluster luminosity drops to 1/3 of its initial value, and t reaches the disk’s dynamical timescale, respectively. *Middle*: The velocity of the swept-up shell. For the vast majority of the evolution, the shell velocity is comparable to the observed velocity dispersion of the gas, $\sim 55 \text{ km s}^{-1}$ (Genzel et al. 2008). *Right*: The forces in our model for the giant clump in BX482, with line styles as in Figure 1.

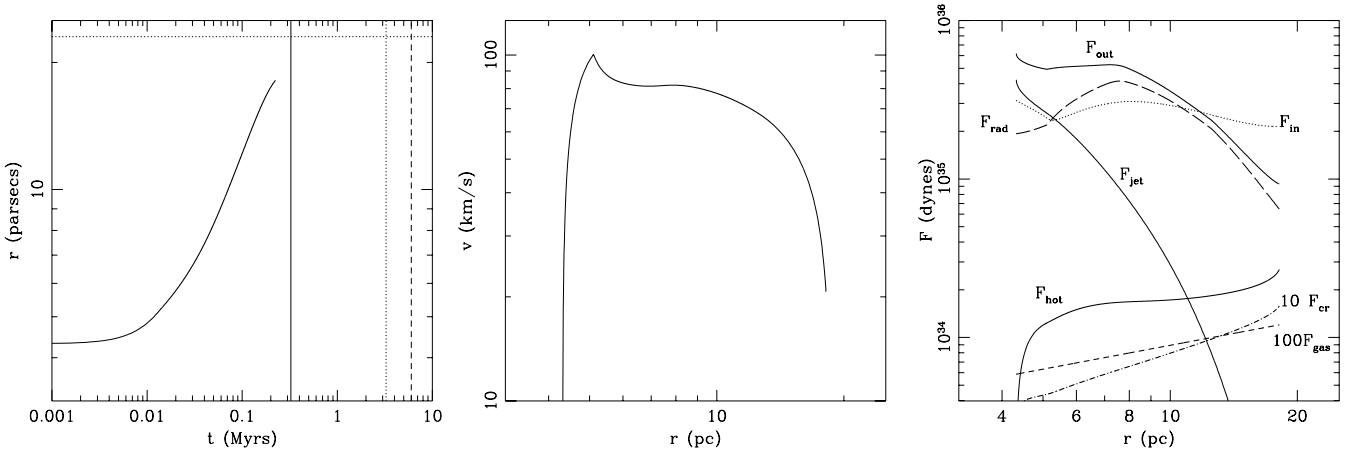


FIG. 4.— *Left*: Bubble radius as a function of time in a model for the disruption of a GMC by a star cluster in the ULIRG Arp 220. The dotted, dashed, and solid lines mark when the first cluster SNe explode, the central cluster luminosity drops to 1/3 of its initial value, and t reaches the disk’s dynamical timescale, respectively. Note that in Arp 220, the disk and GMC dynamical times are short compared to the main sequence lifetime of massive stars, unlike in our other models (see also Table 1). *Middle*: The velocity of the swept-up shell. The upper most solid line is the total outward force F_{out} , consisting of five components: the force exerted by protostellar jets (solid line; F_{jet}), the force exerted by HII gas pressure multiplied by 100 (short dash line; F_{HII}) the force exerted by radiation pressure on dust grains (long dash line; F_{rad}), the force exerted by shocked stellar winds (F_{hot} ; solid), and the force exerted by cosmic-rays produced in stellar wind shocks (F_{cr} ; dot-dashed). Radiation pressure dominates the outward force at nearly all times. The dotted line is the total inward force F_{in} , dominated by the self-gravity of the shell.

where Ψ is the light-to-mass ratio in cgs units. Thus,

$$\frac{F_{\text{sh}}}{F_{\text{rad}}} \sim \frac{\phi_G^2 Gc M_T}{2\Psi H^2} \left(\frac{M_T}{M_*} \right) \sim 1 \left(\frac{3000 \text{ cgs}}{\Psi} \right) \left(\frac{0.02}{\epsilon_{\text{GMC}}} \right) \left(\frac{\Sigma_g}{2 \times 10^{-3} \text{ g cm}^{-2}} \right), \quad (14)$$

where we have scaled to values appropriate to the Galaxy. We see that if ϵ_{GMC} increases with gas surface density, as our calculations indicate (e.g., Table 2), then radiation pressure provides a plausible mechanism for GMC disruption in both spiral galaxies like the Milky Way and somewhat denser and more luminous galaxies.

For galaxies with sufficiently large surface densities, $\Sigma_g \gtrsim 0.5 \text{ g cm}^{-2}$, GMCs will be opaque to the emission by dust in the far-infrared. This increases the radiation pressure force so

that (in the thin shell approximation used here)

$$F_{\text{rad}} = \tau_{\text{rad}} \frac{L}{c} \propto M_* \Sigma_g, \quad (15)$$

where $\tau_{\text{rad}} = \kappa_{\text{FIR}} \Sigma_{\text{sh}} / 2$, κ_{FIR} is the Rosseland mean opacity of the GMC in the FIR and Σ_{sh} is the surface density of material in the shell. Comparing the optically thick radiation pressure force with that due to gravity, we find that

$$\frac{F_{\text{sh}}}{F_{\text{rad}}} \sim \frac{4\pi Gc}{\kappa_{\text{FIR}} \Psi} \left(\frac{M_T}{M_*} \right) \sim 1 \left(\frac{3000 \text{ cgs}}{\Psi} \right) \left(\frac{30 \text{ cm}^2 \text{ g}^{-1}}{\kappa_{\text{FIR}}} \right) \left(\frac{0.25}{\epsilon_{\text{GMC}}} \right), \quad (16)$$

where we have scaled to a relatively high value for the Rosseland-mean dust opacity (see below). Note that the ratio in equation (16) does not explicitly depend on stellar/gas mass, because both F_{sh} and F_{rad} are $\propto M^2$. Using the scalings

in Appendix A, it is easy to see that no other stellar feedback process has this property. Indeed, most of the previously suggested support mechanisms scale as $F \propto M_*^\beta$ with $\beta \leq 1$, viz., HII gas pressure, stellar winds, and pressures associated with shocked stellar winds. For this reason, although many feedback mechanisms are competitive with gravity in normal spirals, the self-gravity of the disk quickly overwhelms the forces due to stellar feedback in starburst galaxies. In contrast to these other feedback processes, radiation pressure in optically thick gas scales as $F_{\text{rad}} \propto M_* M_g$, so that it is at least in principle possible that radiation pressure can disrupt GMCs even in the densest, most gas-rich environments (e.g., ULIRGs and $z \sim 2$ galaxies). Radiation pressure is, to our knowledge, the only stellar feedback process that has this property.

Equation (16) shows that the efficiency of star formation in a GMC at very high densities is sensitive to the metallicity and dust composition, which influence the FIR opacity κ_{FIR} , and to the stellar IMF, which determines the light to mass ratio of the stellar population Ψ . In very dense environments there are some reasons for suspecting that the IMF may be top heavy (e.g., Murray 2009), as appears to be the case in regions of massive star formation more generally (Krumholz et al. 2007). If this is indeed the case, it would increase Ψ and thus decrease the ϵ_{GMC} required for GMC disruption.⁹ For a relatively normal IMF, however, the star formation efficiency in GMCs must be appreciable at high densities, with $\epsilon_{\text{GMC}} \sim 0.25$ or perhaps even larger.

5.2. The FIR Optical Depth

A key part of our argument for the importance of radiation pressure is the fact that star clusters have very high surface densities, which can trap the FIR radiation produced by dust, thus enhancing the radiation force by a factor of $\sim \tau_{\text{rad}}$ in the optically-thick limit (eq. [16]). Figure 5 shows the Rosse-land mean dust optical depth (τ_{rad}) through the shell as a function of radius in the M82 and Arp 220 models (compare with Figs. 2 & 4). In the M82 model, $\tau_{\text{rad}} > 1$ for $r \lesssim 20$ pc, while for Arp 220 $\tau_{\text{rad}} \gg 1$ at all radii. In our Milky Way models, by contrast, we find that the GMC is essentially always in the optically-thin limit, i.e., opaque to the UV but not to the FIR. Figure 5 also shows the *effective optical depth* in both the M82 and Arp 220 models (dashed lines), which we define as

$$\tau_{\text{eff}} \equiv \frac{P_{\text{rad}}}{(L/c)}. \quad (17)$$

The effective optical depth quantifies the enhanced coupling of photons emitted by a cluster in the center of a GMC compared to photons originating at the mid-plane of a uniform density disk. In M82 the effective optical depth at the end of the bubble evolution is about equal to the mean optical depth at the mid-plane. By contrast, in our Arp 220 models, the momentum deposited per photon in the bubble shell is a factor of ~ 3 larger than would be deposited by a photon traversing a uniform density disk. This shows that the effect of the radiation pressure may be three times larger than calculated using the mean mid-plane optical depth, as was done in Thompson et al. (2005). This effect increases the importance of radiation pressure in the densest galaxies, where it

⁹ Note that as IMF becomes arbitrarily top-heavy $\Psi \rightarrow 4\pi Gc/\kappa_T$, where κ_T is the Thomson opacity. This sets a *minimum* on the ratio $F_{\text{sh}}/F_{\text{rad}}$ for any stellar population: $F_{\text{sh}}/F_{\text{rad}}|_{\text{min}} \rightarrow (\kappa_T/\kappa_{\text{FIR}})\epsilon_{\text{GMC}}^{-1} \sim 10^{-2} (30 \text{ cm}^2 \text{ g}^{-1}/\kappa_{\text{FIR}})\epsilon_{\text{GMC}}^{-1}$.

is needed most, effectively decreasing the normalization in equation (16). Note also that because most of the star formation — and thus radiation — occurs in a few massive star clusters in the most massive GMCs (§ 2), there is very little “cancellation” due to different radiation sources driving the gas in different directions (as was suggested by Socrates et al. 2006); the distribution of radiation sources in galaxies is not well-approximated as infinite and homogeneous (§ 2).

Given the turbulent and clumpy nature of the ISM in GMCs, one may question whether or not the photon coupling efficiency is as large as τ_{rad} or τ_{eff} , since these expressions assume uniform shells of matter. We have, after all, used the argument that GMCs are porous to argue that hot gas from shocked stellar winds escapes rapidly from GMCs in the Galaxy. The optical depth τ_{rad} is measured from the center of the protocluster outward and is proportional to the column density of overlying gas; the latter has been observationally measured by a number of authors (e.g., Goodman et al. 2009; Wong et al. 2008) and is consistent with a log-normal distribution. Numerical simulations also find log-normal surface density distributions (Ostriker et al. 2001).¹⁰ In the notation of Ostriker et al. (2001), Goodman et al. (2009) find a dispersion in the logarithm of the column density of $0.11 < \sigma < 0.22$, corresponding to a range of mean logarithmic column densities $0.01 < \mu < 0.05$. This agrees well with the high Mach number turbulence simulations of Ostriker et al. (2001). For $\mu = 0.05$, 99% of sight lines have $\tau/\bar{\tau} \gtrsim 0.5$, where $\bar{\tau}$ is the (angular) mean of the optical depth. There are thus very few optically thin sight lines until the mean optical depth is itself of order unity. This conclusion is based on observations that do not probe, and simulations that do not include, some of the physics relevant to our models (e.g., the Rayleigh-Taylor and photon-bubble instabilities; Blaes & Socrates 2003; Turner et al. 2007; Thompson 2008; Krumholz et al. 2009). Nonetheless, these results provide some support for our argument that the dense ISM will be opaque to FIR radiation, thus significantly enhancing the radiation pressure force in the optically thick limit. In the absence of very large changes in the IMF (Ψ) or the average dust-to-gas ratio (κ_{FIR}), this enhancement is *required* for radiation pressure to disrupt GMCs in dense starbursts. For Milky Way-like galaxies, our conclusions are not sensitive to the radiation force in the optically thick limit, since the GMCs/star clusters are not optically-thick except on very small scales.

5.3. The Origin of Large-Scale Turbulent Motions

In all of our calculations, the shell velocity at $r \approx H_d$ is similar to the turbulent velocity required to maintain Toomre’s $Q \sim 1$ in the ambient disk, thus staving off self-gravity on the largest scales. This is not a coincidence: disrupting the GMC — which we have explicitly taken to be the Toomre mass — requires a force comparable to that needed to stir up the gas in the disk proper to $Q \sim 1$. We have interpreted the shell velocity at large radii as a turbulent velocity because the disruption of the shell by shear, tidal forces, and instabilities (e.g., Rayleigh-Taylor) will inevitably convert this relatively ordered kinetic energy into random fluid motions. More sophisticated models are clearly called for, but it is also clear

¹⁰ The observations measure τ_{rad} along the line of sight from the Earth through the cloud rather than from the center of the cloud outward, but the two surface density distributions should not differ dramatically.

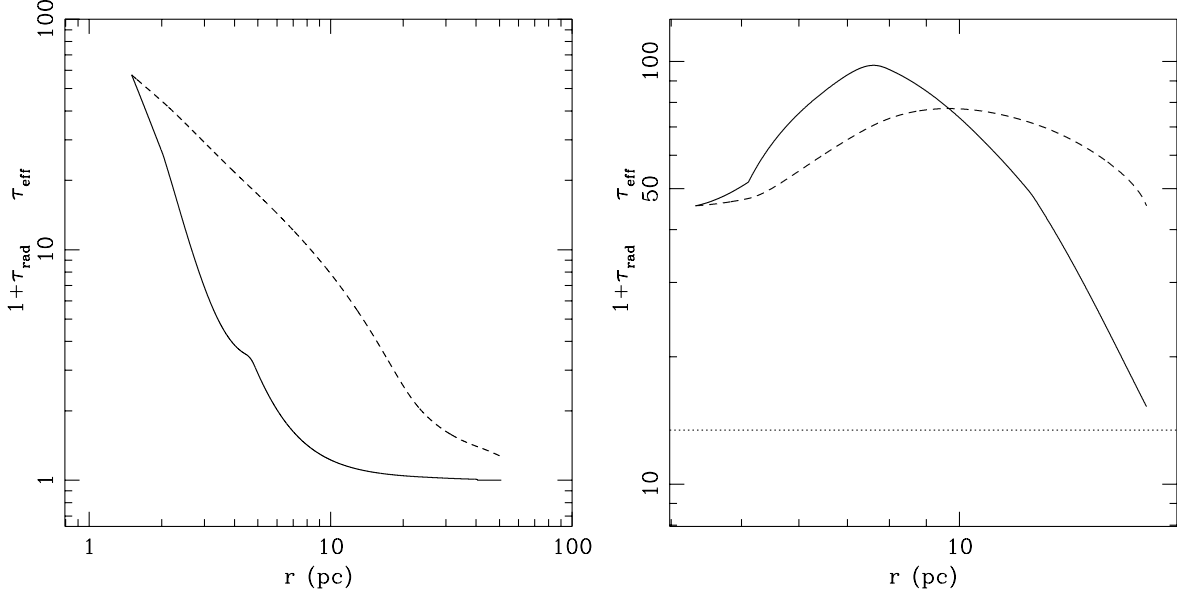


FIG. 5.— The Rosseland mean optical depth ($1 + \tau_{\text{rad}}$) (solid lines) and the effective optical depth τ_{eff} (eq. 17) (dashed lines) as a function of radius in the M82 (left) and Arp 220 (right) models, respectively. Note that τ_{eff} is a factor ~ 3 larger than the mean optical depth of the disk in Arp 220 (the horizontal dotted line), enhancing the magnitude of the radiation pressure force.

that such models must include the effects of radiation pressure, particularly in very optically thick systems like Arp 220, but also in models of Milky Way-like galaxies.

5.4. The Global Star Formation Efficiency in Galaxies

A key question we are unable to fully address is how the efficiency of star formation in a GMC (ϵ_{GMC}) relates to the global star formation rate in the galaxy as a whole, as encapsulated by, e.g., the parameter η in the Kennicutt Law (eq. [1]) or the observed Schmidt Law. We briefly discuss some of the relevant issues here, but leave a more detailed analysis of this problem to future work.

In our models of GMCs in Milky-Way like spirals, the time for a star cluster to disrupt the natal GMC is $1/3$ to $1/2$ the local dynamical time. When we add to this the time for the GMC to contract to its present size, the total time involved will be ~ 2 longer than the local dynamical time of the disk. If the subsequent supernovae do not greatly prolong the process of reincorporating the bulk of the gas back into the disk, which we suspect is correct, the time averaged star formation rate per unit area will be

$$\dot{\Sigma}_* = \epsilon_{\text{GMC}} \Sigma / (2t_{\text{dyn}}) = \eta \Sigma / t_{\text{dyn}}, \quad (18)$$

with η given roughly by $\eta \approx \epsilon_{\text{GMC}}/2 \approx 0.02$, in good agreement with the observations.

The number of clusters capable of disrupting a Toomre mass GMC, in our feedback model, should be proportional to the number of Toomre masses, $\sim (R/H)^2 \sim 700$. The corresponding number of giant HII regions observable at any time is $(R/H)^2 t_{\text{MS}} / (2t_{\text{dyn}}) \approx 30$, where $t_{\text{MS}} \approx 3.6 \times 10^6$ years is the lifetime of an early O star, which is also the time over which a star cluster will emit a large luminosity of ionizing photons.

This estimate is consistent with the fact that half of the free-free emission in the Galaxy is produced by about 17 giant HII regions (Murray & Rahman 2009).

The GMC star formation efficiency is $\epsilon_{\text{GMC}} = 0.38$ for our fiducial Arp 220 model (Table 2); more generally, it is $\epsilon_{\text{GMC}} \sim 0.25$ in the optically thick limit for typical IMFs and dust to gas ratios (eq. [16]). This suggests that η is also ≈ 0.25 , higher than implied by the Kennicutt relation (eq. [1]), although reasonably consistent with the conclusions of Bouché et al. (2007). However, this estimate assumes that after the dispersal of the GMC, gas falls back into the disk and forms a new GMC in a single dynamical time; as the left panel of Figure 4 shows, the timescale for cluster disruption is in fact $\sim 1/10$ of the timescale for the cluster luminosity to drop significantly. Thus, the star cluster luminosity can drive motions in the remaining gas $\sim v_T \sim (H/R)v_c$, sufficient for hydrostatic equilibrium over many (~ 10) dynamical timescales. Because the photon diffusion timescale is rapid compared to the dynamical timescale, the medium cannot be supported stably (Thompson et al. 2005; Thompson 2008). Hydrostatic balance will only be maintained in a statistical sense within a volume $\sim 4H^3$ of the star cluster. After the cluster's luminosity decreases on a timescale $\sim t_{\text{MS}}$ the gas will recollapse to form a new GMC and the process will repeat until gas exhaustion. We suspect that this may reduce η by a factor of $\sim t_{\text{dyn}}/t_{\text{MS}}$, but clearly more work is needed.

We thank Reinhard Genzel and Chris McKee for useful conversations. N.M. is supported in part by the Canada Research Chair program and by NSERC. E.Q. is supported in part by NASA grant NNG06GI68G and the David and Lucile Packard Foundation. T.A.T. is supported in part by an Alfred P. Sloan Fellowship.

REFERENCES

- Blaes, O., & Socrates, A. 2003, *ApJ*, 596, 509
- Blitz, L., Fukui, Y., Kawamura, A., Leroy, A., Mizuno, N., & Rosolowsky, E. 2007, *Protostars and Planets V*, 81
- Bouché, N., et al. 2007, *ApJ*, 671, 303
- Boulares, A., & Cox, D. P. 1990, *ApJ*, 365, 544
- Brandner, W., Clark, J. S., Stolte, A., Waters, R., Negueruela, I., & Goodwin, S. P. 2008, *A&A*, 478, 137
- Bruzual A. G., & Charlot, S. 1993, *ApJ*, 405, 538
- Castor, J., McCray, R., & Weaver, R. 1975, *ApJ*, 200, L107
- Chevalier, R. A., & Fransson, C. 2001, *ApJ*, 558, L27
- Chiao, R. Y., & Wickramasinghe, N. C. 1972, *MNRAS*, 159, 361
- Chu, Y.-H., & Mac Low, M.-M., 1990, *ApJ*, 365, 510
- Crowther, P. A., Hadfield, L. J., Clark, J. S., Negueruela, I., & Vacca, W. D. 2006, *MNRAS*, 372, 1407
- Dorland, H. & Montmerle, T. 1987, *A&A*, 177, 243
- Downes, D. & Solomon, P. M. 1998, *ApJ*, 507, 615
- Evans, N. J., II, et al. 2008, arXiv:0811.1059
- Elmegreen, B. G. 1983, *MNRAS*, 203, 1011
- Elmegreen, B. G. 2009, *The Evolving ISM in the Milky Way and Nearby Galaxies*, 14
- Elmegreen, B. G. & Efremov, Y. N. 1997, *ApJ*, 480, 235
- Engargiola, G., Plambeck, R. L., Rosolowsky, E., & Blitz, L. 2003, *ApJS*, 149, 343
- Evstigneeva, E. A., Gregg, M. D., Drinkwater, M. J., & Hilker, M. 2007, *AJ*, 133, 1722
- Ferrara, A. 1993, *ApJ*, 407, 157
- Figier, D. F., Kim, S. S., Morris, M., Serabyn, E., Rich, R. M., & McLean, I. S. 1999, *ApJ*, 525, 750
- Figier, D. F. et al. 2006, *ApJ*, 643, 1166
- Freedman, W. L., et al. 1994, *ApJ*, 427, 628
- Fukui, Y., et al. 2008, *ApJS*, 178, 56
- Gardner, F. F., Milne, D. K., Metzger, P. G., & Wilson, T. L. 1970, *A&A*, 7, 349
- Geha, M., Guhathakurta, P., & van der Marel, R. P. 2002, *AJ*, 124, 3073
- Genzel, R., et al. 2008, *ApJ*, 687, 59
- Goodman, A. A., Pineda, J. E., & Schnee, S. L. 2009, *ApJ*, 692, 91
- Grabelsky, D. A., Cohen, R. S., Bronfman, L. & Thaddeus, P. 1988, *ApJ*, 331, 181
- Harper-Clark, E., & Murray, N. 2009, *ApJ*, 693, 1696
- Harris, W. E. 1996, *AJ*, 112, 1487
- Hasegan, M., et al., 2005, *ApJ*, 627, 203
- Hilker, M., Baumgardt, H., Infante, L., Drinkwater, M., Evstigneeva, E., & Gregg, M. 2007, *A&A*, 463, 119
- Keto, E., Ho, L. C., & Lo, K.-Y. 2005, *ApJ*, 635, 1062
- Kennicutt, R. C. 1989, *ApJ*, 344, 685
- Kennicutt, R. C., Jr., Edgar, B. K., & Hodge, P. W. 1989, *ApJ*, 337, 761
- Kondratko, P. T., Greenhill, L. J., & Moran, J. M. 2005, *ApJ*, 618, 61
- Kothes, R., & Dougherty, S. M. 2007, *A&A*, 468, 993
- Krumholz, M. R., & McKee, C. F. 2005, *ApJ*, 630, 250
- Krumholz, M. R., Matzner, C. D., & McKee, C. F. 2006, *ApJ*, 653, 361
- Krumholz, M. R., Klein, R. I., & McKee, C. F. 2007, *ApJ*, 656, 959
- Krumholz, M. R., Klein, R. I., McKee, C. F., Offner, S. S. R., & Cunningham, A. J. 2009, *Science*, 323, 754
- Lada, C. J., & Lada, E. A. 2003, *ARA&A*, 41, 57
- Laor, A., & Draine, B. T. 1993, *ApJ*, 402, 441
- Leroy, A. K., Walter, F., Brinks, E., Bigiel, F., de Blok, W. J. G., Madore, B., & Thornley, M. D. 2008, arXiv:0810.2556
- Lynds, C. R., & Sandage, A. R. 1963, *ApJ*, 137, 1005
- Mac Low, M.-M. 1999, *ApJ*, 524, 169
- Matzner, C. D., & McKee, C. F. 2000, *ApJ*, 545, 364
- Matzner, C. D. 2002, *ApJ*, 566, 302
- McCraday, N., Gilbert, A. M., & Graham, J. R. 2003, *ApJ*, 596, 240
- McCraday, N., & Graham, J. R. 2007, *ApJ*, 663, 8
- McKee, C. F., & Ostriker, E. C. 2007, *ARA&A*, 45, 565
- McKee, C. F., Van Buren, D., & Lazareff, B. 1984, *ApJ*, 278, 115
- McKee, C. F., & Williams, J. P. 1997, *ApJ*, 476, 144
- Melo, V. P., Muñoz-Tuñón, C., Maíz-Apellániz, J., & Tenorio-Tagle, G. 2005, *ApJ*, 619, 270
- Mengel, S., & Tacconi-Garman, L. E. 2007, *A&A*, 466, 151
- Munch, A. A., Lada, E. A., Lada, C. J., & Alves, J. 2002, *ApJ*, 573, 366
- Muno, M. P., Law, C., Clark, J. S., Dougherty, S. M., de Grijs, R., Portegies Zwart, S., & Yusef-Zadeh, F. 2006, *ApJ*, 650, 203
- Muno, M. P., et al. 2006, *ApJ*, 636, L41
- Murray, N., 2009 *ApJ*, 691, 946
- Murray, N. W., & Rahman, M. 2009, arXiv:0906.1026
- Murray, N., Quataert, E., & Thompson, T. A. 2005, *ApJ*, 618, 5
- Nakamura, F. & Li, Z.-Y. 2007, *ApJ*, 662, 395
- O'Dell, C. R., York, D. G., & Henize, K. G. 1967, *ApJ*, 150, 835
- Oey, M. S. 1996, *ApJ*, 467, 666
- Ostriker, E. C., Stone, J. M., & Gammie, C. F. 2001, *ApJ*, 546, 980
- Parker, E. N. 1969, *Space Science Reviews*, 9, 651
- Pellegrini, E. W., et al. 2007, *ApJ*, 658, 1119
- Pellegrini, E. W., Baldwin, J. A., Ferland, G. J., Shaw, G., & Heathcote, S. 2009, *ApJ*, 693, 285
- Press, W. H., Teukolsky, S. A., Vetterling, W. T., & Flannery, B. P. 1992, *Cambridge: University Press*, |c1992, 2nd ed.
- Pryor, C., & Meylan, G. 1993, *Structure and Dynamics of Globular Clusters*, 50, 357
- Quirk, W. J. 1972, *ApJ*, 176, 9
- Ranalli, P., Comastri, A., & Setti, G. 2003, *A&A*, 399, 39
- Rauw, G., Nazé, Y., Gosset, E., Stevens, I. R., Blomme, R., Corcoran, M. F., Pittard, J. M., & Runacres, M. C. 2002, *A&A*, 395, 499
- Rejkuba, M., Dubath, P., Minniti, D., & Meylan, G. 2007, *A&A*, 469, 147
- Robishaw, T., Quataert, E., & Heiles, C. 2008, *ApJ*, 680, 981
- Sakamoto, K., Scoville, N. Z., Yun, M. S., Crosas, M., Genzel, R., & Tacconi, L. J. 1999, *ApJ*, 514, 68
- Salpeter, E. E. 1955, *ApJ*, 121, 161
- Sanders, D. B., Mazzarella, J. M., Kim, D.-C., Surace, J. A., & Soifer, B. T. 2003, *AJ*, 126, 1607
- Scheepmaker, R. A., Haas, M. R., Gieles, M., Bastian, N., Larsen, S. S., & Lamers, H. J. G. L. M. 2007, *ArXiv e-prints*, 704, arXiv:00704.3604
- Schlickeiser, R. 2002, *Cosmic ray astrophysics / Reinhard Schlickeiser, Astronomy and Astrophysics Library; Physics and Astronomy Online Library*. Berlin: Springer. ISBN 3-540-66465-3, 2002, XV + 519 pp.
- Scoville, N. Z., Polletta, M., Ewald, S., Stolovy, S. R., Thompson, R., & Rieke, M. 2001, *AJ*, 122, 3017
- Scoville, N. 2003, *Journal of Korean Astronomical Society*, 36, 167
- Sellwood, J. A., & Balbus, S. A. 1999, *ApJ*, 511, 660
- Semenov, D., Henning, T., Helling, C., Ilgner, M., & Sedlmayr, E. 2003, *A&A*, 410, 611
- Seward, F. D., Forman, W. R., Giacconi, R., Griffiths, R. E., Harnden, F. R., Jones, C., & Pye, J. P. 1979, *ApJ*, 234, L55
- Shen, J., & Lo, K. Y. 1996, *CO: Twenty-Five Years of Millimeter-Wave Spectroscopy*, 170, 101P
- Smith, N. 2006, *MNRAS*, 367, 763
- Smith, L. J., & Gallagher, J. S. 2001, *MNRAS*, 326, 1027
- Smith, B. J., Struck, C., & Nowak, M. A. 2005, *AJ*, 129, 1350
- Smith, L. J., Westmoquette, M. S., Gallagher, J. S., O'Connell, R. W., Rosario, D. J., & de Grijs, R. 2006, *MNRAS*, 370, 513
- Socrates, A., Davis, S. W., & Ramirez-Ruiz, E. 2006, arXiv:astro-ph/0609796
- Solomon, P. M., Rivolo, A. R., Barrett, J., & Yahil, A. 1987, *ApJ*, 319, 730
- Spoon, H. W. W., Moorwood, A. F. M., Lutz, D., Tielens, A. G. G. M., Siebenmorgen, R., & Keane, J. V. 2004, *A&A*, 414, 873
- Thompson, T. A., Quataert, E., & Murray, N. 2005, *ApJ*, 630, 167
- Thompson, T. A., Quataert, E., Waxman, E., Murray, N., & Martin, C. L. 2006, *ApJ*, 645, 186
- Thompson, T. A. 2008, *ApJ*, 684, 212
- Thornton, K., Gaudlitz, M., Janka, H.-T., & Steinmetz, M. 1998, *ApJ*, 500, 95
- Tsujimoto, M., Hosokawa, T., Feigelson, E. D., Getman, K. V., & Broos, P. S. 2006, *ApJ*, 653, 409
- Turner, N. J., Quataert, E., & Yorke, H. W. 2007, *ApJ*, 662, 1052
- van den Bergh, S. & Lafontaine, A. 1984, *AJ*, 89, 1822
- Walcher, C. J., et al., 2005 *ApJ*, 618, 237
- Weaver, R., McCray, R., Castor, J., Shapiro, P., & Moore, R. 1977, *ApJ*, 218, 377
- Weiß, A., Neiningner, N., Hüttemeister, S., & Klein, U. 2001, *A&A*, 365, 571
- Williams, J. P., & McKee, C. F. 1997, *ApJ*, 476, 166
- Wilson, C. D., Harris, W. E., Longden, R., & Scoville, N. Z. 2006, *ApJ*, 641, 763
- Wong, T., et al., 2008 *MNRAS*, 386, 1069
- Yonekura, Y., Asayama, S., Kimura, K., Ogawa, H., Kanai, Y., Yamaguchi, N., Barnes, P. J., & Fukui, Y. 2005, *ApJ*, 634, 476
- Young, J. S., & Scoville, N. Z. 1984, *ApJ*, 287, 153

APPENDIX

FORCES INCLUDED IN THE MODELS

In this section we describe the forces acting on gas surrounding massive star clusters embedded in giant molecular clouds.

*Inward Forces**Gravity*

We assume that the gravitational force acting on the bubble shell consists of three components, $F_{\text{grav}} = F_{\text{stars}} + F_{\text{shell}} + F_{\text{disk}}$. The central star cluster exerts a force on the bubble shell given by

$$F_{\text{stars}} = -\frac{GM_*M_{\text{sh}}}{r^2}, \quad (\text{A1})$$

the shell self-gravity is

$$F_{\text{shell}} = -\frac{GM_{\text{sh}}^2}{2r^2}, \quad (\text{A2})$$

while the mass in the galactic disk exerts a force

$$F_{\text{disk}} = -\frac{v_c^2 M_{\text{sh}}}{R_d} \frac{r}{R_d}. \quad (\text{A3})$$

The last force is that exerted on the part of the shell rising vertically away from the disk; gas in the plane of the disk will not feel this force, but we ignore this complication, just as we ignore Coriolis forces.

Ram Pressure

As the shell expands into the ISM of the galaxy it will sweep up gas. This swept up gas exerts a ram pressure on the shell giving a force

$$F_{\text{ram}} = -\frac{dM_{\text{sh}}}{dr} v^2, \quad (\text{A4})$$

where dM/dr is given by the appropriate derivative of equation (7) or (8).

Turbulent Pressure

The pressure in the interstellar medium and in the GMC provides an inward force on the shell. We refer to these pressures as turbulent pressure, although there may be other components such as magnetic or cosmic ray pressure. We approximate them as

$$F_{\text{turb}} = -4\pi r^2 P_{\text{ISM}} - \frac{GM_{\text{GMC}}^2}{R_{\text{GMC}}^2} \left[1 - \left(\frac{r}{R_{\text{GMC}}} \right)^2 \right]. \quad (\text{A5})$$

Here we have assumed that the GMC has a Larson-like mass distribution. A similar expression holds for clouds with $\rho(r) \sim 1/r^2$. The pressure of the ISM is given by

$$P_{\text{ISM}} \approx \pi G \Sigma_d^2. \quad (\text{A6})$$

*Outward Forces**Gas Pressure Forces*

The large luminosity Q (number per second) of ionizing photons produced by the massive stars in a young star cluster will photoionize and heat gas in the vicinity of the cluster, raising the gas pressure above that in the neutral gas. This hot gas will exert an outward force on the bubble wall, with a magnitude

$$F_{\text{HII}} = 4\pi r^2 P_{\text{HII}} \quad (\text{A7})$$

The gas pressure is taken to be

$$P_{\text{HII}} = nkT \quad (\text{A8})$$

where $T = 8000\text{K}$ (Gardner et al. 1970) and

$$n = \sqrt{\frac{Q}{\alpha_{\text{rec}} V}}. \quad (\text{A9})$$

The volume $V = 4\pi r^3/3$ and the recombination coefficient $\alpha_{\text{rec}} \approx 4 \times 10^{-13}$. In models for clusters in the Milky Way, the shell velocity is subsonic, so the gas pressure is roughly constant throughout the bubble. If there is any hot gas or cosmic rays due to,

for example, shocked stellar winds, they will also be roughly isobaric, and in pressure equilibrium with the HII gas. If the hot gas or cosmic ray pressure is in excess of the estimate given here, the HII gas will be confined to a fraction of the bubble volume. However, observations of Carina and massive Milky Way and LMC clusters suggest that the pressure is well approximated by (A8) and (A9) (Harper-Clark & Murray 2009).

For large enough stellar clusters, those with at least one $35M_{\odot}$ star, Q is proportional to L ,

$$\frac{L}{Q} \equiv \xi \approx 8 \times 10^{-11} \text{ erg}, \quad (\text{A10})$$

or about 3.6 Rydbergs ($1\text{Ryd} \approx 2.2 \times 10^{-11}$ is the energy required to ionize hydrogen). The HII gas pressure inside the bubble is then

$$P_{\text{HII}} = 5.0 \times 10^{-10} \left(\frac{L}{10^{41}} \right)^{1/2} \left(\frac{5 \text{ pc}}{r} \right)^{3/2} \left(\frac{T}{8000\text{K}} \right) \text{ dynes cm}^{-2}, \quad (\text{A11})$$

assuming a unit filling factor for the HII gas, i.e., ignoring the hot shocked winds.

It is helpful to have an estimate for n in terms of the luminosity. The number density $n(L, r)$ is given by

$$n(L, r) = \sqrt{\frac{3L}{4\pi\alpha\xi r^3}}. \quad (\text{A12})$$

If the bubble is breached, so that HII gas leaks out, the pressure in the bubble will be lower than the estimate given here, but the force experienced by the bubble wall will actually be larger. The reason is that fewer ionizing photons are absorbed in the bubble cavity, leaving more to heat the gas on the interior of the bubble wall. The heated gas escapes away from the wall into a partial vacuum, exerting a force

$$F = \dot{M}c_{\text{HII}} \quad (\text{A13})$$

on the wall. The mass loss rate is given by $4\pi r^2 m_p n c_{\text{HII}}$. In our numerical work we have assumed that the HII gas leaks out of the bubble, since the rapidly expanding ionized gas at the ionization front will exert a larger force, and we want an upper limit on the efficacy of HII gas pressure.

In models for ULIRGs like Arp 220, the bubble expansion velocity is larger than the sound speed of 8000 K gas, so the HII pressure may be twice that in the subsonic case even if no gas escapes from the bubble. However, the pressure associated with HII gas is negligible in ULIRGs, as we show in the main text.

Forces Associated With Shocked Stellar Winds

Hot gas from shocked stellar winds is often thought to be important in the formation of bubbles around massive stars or star clusters. We argue here that it is not; see also Harper-Clark & Murray (2009). We further argue that cosmic ray pressure cannot be important in Milky Way bubbles; if they were, the bubbles would expand more rapidly than is observed. We show in this paper that neither hot gas nor cosmic ray pressure is not relevant in ULIRGs.

The force due to hot, shocked stellar wind gas: X-Ray Constraints

O stars emit high velocity massive winds; in clusters these winds are seen to shock and emit diffuse x-rays at \sim KeV energies (Seward et al. 1979; Oey 1996; Smith, Struck, & Nowak 2005). If the stellar winds are confined to the bubble interior, the associated pressure can be far larger than the ram pressure of the wind (Castor et al. 1975). The force is given by

$$F_h = 4\pi r^2 P_h, \quad (\text{A14})$$

where $P_h = 2E_h/(3V)$. The energy equation for the hot gas is

$$\frac{dE_h}{dt} = L_w - 4\pi r^2 P_h v_{\text{sh}} - \Lambda n_h^2 V; \quad (\text{A15})$$

recall that V is the volume of a bubble of radius r and Λ is the cooling function. The wind luminosity $L_w = (1/2)\eta(v_{\infty}/c)L_{\text{bol}}$, ($\eta \approx 0.5$ is the fraction of stellar luminosity scattered in the wind) and L_{bol} is the bolometric luminosity of the cluster.

We follow Castor et al. (1975) to find the number density n_h of hot gas, i.e., we assume that heat conduction (at the Spitzer rate $C_{\text{Sp}} T_h^{5/2}$) drives a mass flow into the bubble interior (possibly supplemented from cold gas clouds in the interior of the bubble) at a rate

$$\frac{dM_h}{dt} = \frac{16\pi m_p C_{\text{Sp}} T_h^{5/2} r}{25k}. \quad (\text{A16})$$

Given E_h and the radius of the bubble we find the hot gas pressure; from equation (A16) we find n_h , and hence the temperature. With n_h and T_h , we can find the cooling rate (the third term on the right hand side of the energy equation (A15)).

The solar-mass stars in clusters also emit x-rays; in low resolution (non-Chandra) observations, these stars appear as diffuse emission, so care must be taken to distinguish the two. Assuming that one can extract the stellar emission, the diffuse x-ray flux

can be used to constrain the pressure of any hot gas component. Harper-Clark & Murray (2009) use this to show that for clusters in the Milky Way and the LMC, the x-ray gas is in approximate pressure equilibrium with the HII gas, and that the HII gas has a filling factor near unity (greater than ~ 0.1). The implication is that the shocked winds either radiate away the bulk of their energy, or else leak out of the bubble wall. In either case, they do not play any role in the dynamics of the bubble, a conclusion also reached by McKee, Van Buren, & Lazareff (1984).

Harper-Clark & Murray (2009) show that observations of ultracompact HII regions (Rauw et al. 2002; Tsujimoto et al. 2006) reveal a similar story.

If the bubbles that form around star clusters in ULIRGs are also leaky, the shocked wind pressure would be negligible, as in the Milky Way. However, even if we assume that the winds are perfectly trapped, the high ambient pressures in ULIRGs ensure that the shocked gas is not dynamically important.

To see this, note that we expect a total number of young (ionizing) clusters in a ULIRG to be

$$N_{\text{cl}} = \left(\frac{R}{H}\right)^2 \approx 20. \quad (\text{A17})$$

If there are ~ 20 clusters powering Arp 220, each must have $L_{\text{cl}} \approx 5 \times 10^{10} L_{\odot}$, and a mass $M_{\text{cl}} \approx 2 \times 10^7 M_{\odot}$ assuming a normal (Muench et al. 2002) IMF; this cluster luminosity is also that needed to disrupt a GMC in Arp 220, as we showed in §4.4. The wind luminosity of a single such cluster is $L_w \approx 7 \times 10^{41} \text{ erg s}^{-1}$. We note that $L_{\text{cl}} \approx 5 \times 10^{10}$ is about 3–4 times the luminosities of known young star clusters in Arp 220 (Wilson et al. 2006).

From Figure 4 the bubble disrupts the GMC ($R_{\text{GMC}} \approx 10 \text{ pc}$) after a time $t \sim 5 \times 10^{12} \text{ s}$. Assuming no losses, the wind energy accumulated in the bubble is $E_h = 2.5 \times 10^{54} \text{ erg}$. The pressure is $2E_h/3V = 10^{-5} \text{ dynes cm}^{-2}$, about equal to the ambient pressure in the disk but well below the radiation pressure, $\tau F/c \approx 10^{-4} \text{ dynes cm}^{-2}$.

The force we have estimated from the hot gas is $1.6 \times 10^{35} \text{ dynes}$; in the right panel of Figure 4 the force from the hot gas is a factor of ~ 5 below this estimate. The reason is that the hot gas suffers radiative losses, so that we have overestimated E_h . We note that in our numerical work we have assumed that the hot gas fills the volume of the bubble; if it does not, the cooling rate will be higher than we have calculated.

The force due to wind generated cosmic rays

In addition to producing hot gas, wind shocks will generate cosmic rays. Perhaps a third of the wind energy may be expected to be deposited into cosmic rays. If, as observed in the Milky Way, the hot gas is advected out of the shell, it will probably take the cosmic rays with it, so that both the hot gas and the cosmic rays are not dynamically relevant.

We note that the pressure due to cosmic rays, if perfectly confined, would be 1/6 that of similarly confined shocked winds. As noted in the introduction, the dynamics of bubbles in the Milky Way and the LMC are not consistent with the high pressures associated with trapped hot gas; it follows that cosmic rays are probably also not confined to the interiors of such bubbles.

If the shocked winds in ULIRGs also flow through the swept up shell, cosmic rays are unlikely to be dynamically important. Even if the cosmic rays are confined, the cosmic ray pressure is still negligible. The cluster bolometric luminosity is $2 \times 10^{44} \text{ erg s}^{-1}$, so the wind luminosity is $5 \times 10^{41} \text{ erg s}^{-1}$. Assuming 1/3 of this is deposited in cosmic rays, the cosmic ray luminosity is $L_{\text{cr}} \approx 1.6 \times 10^{41} \text{ erg s}^{-1}$. The cosmic ray pressure when the bubble radius is 10 pc is

$$P_{\text{cr}} = \frac{L_{\text{cr}} t_{\text{dyn}}}{V} \approx 7 \times 10^{-6} \left(\frac{\text{pc}}{R_{\text{GMC}}}\right)^3 \text{ dynes cm}^{-2}. \quad (\text{A18})$$

This is about a half of the mean dynamical pressure in the galaxy, but only several percent of the dynamical pressure in the bubble. This is still likely to be an overestimate of the cosmic ray pressure, as cosmic rays will quickly diffuse out of the bubble. The cosmic ray mean free path in the Milky Way is $0.1 \text{ pc} < \lambda_{\text{cr}} < 1 \text{ pc}$ (Schlickeiser 2002); scaling to the lower value, the time for a cosmic ray to diffuse out of a GMC in Arp 220 is

$$t_{\text{cr}} = \frac{R_{\text{GMC}}^2}{D_{\text{cr}}} \approx 2 \times 10^{11} \left(\frac{0.1 \text{ pc}}{\lambda_{\text{cr}}}\right) \text{ s}, \quad (\text{A19})$$

where $D_{\text{cr}} = \lambda_{\text{cr}} c/3$ is the cosmic ray diffusion coefficient. This diffusion time is ~ 10 – 20 times shorter than the bubble dynamical time, so even if the mean free path for cosmic rays in Arp 220 is substantially smaller than in the Milky Way, cosmic rays will diffuse out of the bubbles in the ULIRG. Figure 4 shows that the cosmic ray pressure is a little less than one percent of the radiation pressure; the lower cosmic ray pressure is the result of taking $P_{\text{cr}} = L_{\text{cr}} t_{\text{cr}}/V$, which accounts for diffusive losses, instead of equation (A18). Note that we have optimistically ignored cosmic ray losses due to inelastic proton-proton collisions, which cool the cosmic ray population with energies $\gtrsim \text{GeV}$ on a timescale $t_{\text{pp}} \approx 5 \times 10^3 (10^4 \text{ cm}^{-3}/n) \text{ yr}$, where we have scaled to the average volumetric gas density of Arp 220.

Protostellar Jets

While stars are actively accreting in the protocluster, we assume that they will emit high velocity outflows or jets. Once the cluster disrupts, the accretion halts, and the jets turn off. We assume that this happens over a time given by ϕ_{ff} times t_{ff} of the

cluster; in addition, we allow for an extra factor of two to account for the fact that the accretion disks will not vanish once the cluster gas is dissipated, but instead will accrete onto the star in a disk viscous time:

$$t_{\text{jet}} = 2\phi_{\text{ff}}t_{\text{ff}}. \quad (\text{A20})$$

We take $\phi_{\text{ff}} = 3$. The jets deposit momentum into the surrounding gas at a rate

$$F_{\text{jet}} = \epsilon_{\text{jet}}\dot{M}_{\text{acc}}v_{\text{jet}}\exp^{-t/t_{\text{jet}}} \quad (\text{A21})$$

The jets expel mass at a fraction $\epsilon_{\text{jet}} \approx 0.1 - 0.3$ of the mass accretion rate (Matzner & McKee 2000), at a velocity v_{jet} that depends on the mass of the star. We estimate v_{jet} by calculating the escape velocity from the surface of a star of mass m , using the radius of a star of that mass found from the main sequence radius as given by the Padova models; this is a slight over estimate of the escape velocity, since accreting stars are larger than main sequence stars, but we compensate for this by using the escape velocity rather than the (larger) terminal velocity of a wind or jet. We then average over the initial mass function to yield v_{jet} . For a Muench et al. IMF we find $v_{\text{jet}} \approx 3 \times 10^7 \text{ cm s}^{-1}$, but for top heavy IMFs this can increase to 10^8 cm s^{-1} . We varied ϵ_{jet} over the range $0.1 - 0.3$ giving an effective velocity in the range $30 - 90 \text{ km s}^{-1}$, bracketing that found by, e.g., Matzner & McKee (2000) and Nakamura & Li (2007). The results did not depend strongly on this parameter, but because the clusters we consider are so dense, we expect a substantial amount of momentum cancellation (from jets colliding nearly head on) we used low values for ϵ_{jet} in the runs presented here.

Radiation Force

The radiation force is given by

$$F_{\text{rad}} = (1 + \tau_{\text{rad}})\frac{L}{c}, \quad (\text{A22})$$

where τ_{rad} is the Rosseland mean opacity through the shell. The gas in the shell has a temperature that is of order 100K, so for most clusters in the Milky Way $\tau_{\text{rad}} < 1$. We calculate the optical depth as follows: we assume the shell has a thickness $1/10$ of its radius, and divide it into 100 pieces. We assume that the density is constant through the shell. We calculate T_{eff} from L and the radius r of the shell. Given T and ρ , we use the opacity tables of Semenov et al. (2003) to find the Rosseland mean opacity in the outermost slice of the shell. Subsequently we find the optical depth, then integrate the radiative transfer equations inward through the shell. The factor of unity in equation (A22) accounts for the fact that the temperature of the radiation field is of order 30,000K at the inside edge of the shell, before the photons have encountered any dust grains; upon striking a dust grain, the photons provide an impulse per unit time given by L/c .